JCAMECH

Vol. 49, No. 1, June 2018, pp 102-124
DOI: 10.22059/jcamech.2018.249468.227

Free vibration and buckling analysis of third-order shear deformation plate theory using exact wave propagation approach

A.Zargaripoor[a], A.Bahrami[b], M.Nikkhah Bahrami [a]*

[a] School of Mechanical Engineering, College of Engineering, University of Tehran, Tehran, Iran
[b] Department of Mechanical Engineering, Eastern Mediterranean University, Magosa, TRNC Mersin 10, Turkey

ARTICLE INFO

Article history:
Received: *03 January 2018*
Accepted: *20 January 2018*

Keywords:
Rectangular thick plate
Propagation matrix
Reflection matrix
Vibration analysis
Buckling analysis

ABSTRACT

In this paper, wave propagation approach is used to analysis the free vibration and buckling analysis of the thick rectangular plates based on higher order shear deformation plate theory. From wave viewpoint, vibrations can be considered as travelling waves along structures. Waves propagate in a waveguide and reflect at the boundaries. It is assumed that the plate has two opposite edge simply supported while the other two edges may be simply supported or clamped. It is the first time that the wave propagation method is used for thick plates. In this study, firstly the matrices of propagation and reflection are derived and by combining them, the characteristic equation of the plate is obtained. Comprehensive results on dimensionless natural frequencies and dimensionless buckling loads of rectangular thick plates with different boundary conditions for various values of aspect ratio and thickness to length ratio are presented. It is observed that obtained results of wave propagation method with considerable accuracy are so close to obtained values by literature.

1. Introduction

Due to the many uses they have in different structures, plates have always been of great importance for researchers in various sciences. To model dynamic and static behavior of plates, there are different theories. These theories are based on assumptions, limitations, benefits, and applications. The most common theories used, with regard to the plates, include the classical theory of thin plates known as the Kirchhoff theory [1] the first-order shear deformation plate theory known as Mindlin theory [2] and the third-order shear deformation plate theory known as Reddy theory [3]. Regularly, a thin plate is a plate that the ratio of its thickness to its lateral dimensions is 1/20 or less. In practice, most plates satisfy this condition, which makes it possible to use the classical theory of thin plates to obtain the fundamental frequency (lowest frequency) of most plates. However, the second frequency of the plate with a thickness of 1/20 will not be accurate with this theory and the error will be relatively high. For higher frequencies, this error increases. This theory can be considered as the generalized version of Euler–Bernoulli beam theory. In this theory, it is assumed that each section of the plate, after the application of force, remains in the form of a plate flat and perpendicular to the neutral plate or the middle plate [4].The shear stresses and strains are ignored. This theory can be considered as the simplest theory used in modeling the behavior of plates. The field of validity of this theory is limited to thin plates. Recently, some of problems with thin plates have been solved with Kirchhoff theory assumptions.

Bell [5] presented the derivation of stiffness matrix for a refined, fully compatible triangular plate bending finite element.Liew and Liu [6] presented a treatment for bending analysis of Kirchhoff plates using the differential cubature method. Wei, Zhao and Xiang [7] introduces the discrete singular convolution algorithm for vibration analysis of rectangular plates with mixed boundary conditions. Lu et al. [8] used the differential quadrature method based on the state-space formalism for vibration analysis of generally supported rectangular Kirchhoff plates. Papargyri-Beskou and Beskos [9] derived the government equation of motion of gradient elastic flexural Kirchhoff plates, including the effect of in-plane constant forces on bending. Dozio [10] presented a comprehensive study on the use of a set of trigonometric functions, as admissible solutions in Ritz method for general vibration analysis of rectangular orthotropic Kirchhoff plates. Shojaee et al. [11] presented an isogeometric finite element method for natural frequencies analysis of thin plate problems of various geometries. Brenner et al. [12] studied a Morley finite element method for the displacement obstacle problem of clamped Kirchhoff plates on polygonal domains. Millar and Mora [13] developed a finite element method to approximate the buckling problem of simply supported Kirchhoff plates subjected to general plane stress tensor. Cetkin and Orak [14] employed the hybrid approach of the

* Corresponding Author. . Tel.: +98 126064537; Fax: +98 21 44648239 *Email Address*: alizargaripoor@ut.ac.ir

quadrature element method to generate solutions for point supported isotropic plates.

Although classical theory of plates predicts the frequency of thin plates, it does not consider the effect of transverse shear deformation. In Mindlin and Reddy theories, the bending effect caused by shear deformation and the impact of moment of inertia were considered. Therefore, the little precision of Kirchhoff assumptions was solved in Mindlin and Reddy theories since these two factors increase the frequency. Also, in the third order shear deformation plate theory, after expanding the displacement relations up to the third order along the thickness, some equations consisting of the third order variables including relations of the transverse shear stresses and strains are obtained. This eliminates the necessity of using the shear correction coefficient of the first-order shear theory. In recent years, a lot of researches have been done on moderately thick and thick plates.

Reddy and Khdeir [15] developed an analytical and finite-element solutions of the classical, first-order, and third-order laminated theories to study the buckling and free-vibration behavior of cross-ply rectangular composite laminates under various boundary conditions. Shen et al. [16] presented free and forced vibration analysis for Reissner-Mindlin plates with four free edge resting on a Pasternak-type elastic foundation. Qian, et al. [17] used a meshless local Petrov-Galerkin method to analyze three-dimensional infinitesimal elastodynamic deformations of a homogeneous rectangular plate subjected to different edge conditions. Hosseini Hashemi and Arsanjani [18] derived the dimensionless equations of motion based on the mindlin plate theory to study the transverse vibration of thick rectangular plates. Shi [19] presented an improved simple thire-order shear deformation theory for the analysis of shear flexible plates. Hosseini-Hashemi et al. [20] used the Mindlin plate theory to study buckling of in-plane isotropic rectangular plates with different boundary conditions. Hosseini-Hashemi et al. [21] presented an exact closed-form solutions in explicit forms for transverse vibration analysis of rectangular thick plates having two opposite edge hard simply supported based on Reddy's third-order shear deformation plate theory. Eftekhari and jafari [22] proposed a simple mixed Ritz-differential quadrature (DQ) methodology for free and forced vibration, and buckling analysis of rectangular plates. Dongyan Shi, et al. [23] presented a generalized Fourier series solution based on the first-order shear deformation theory for free vibration of moderately thick rectangular plates with variable thickness and arbitrary boundary conditions. Pradhan and Chakraverty [24] investigated the four new inverse trigonometric shear deformation theories to study free vibration characteristics of isotropic thick rectangular plates subjected to various boundary conditions. Senjanovic et al. [25] presented a new procedure for determining properties of thick plate finite elements, based on the modified Mindlin theory for moderately thick plate. Xiang and Xing [26] presented a new first-order shear deformation theory with pure bending deflection and shearing deflection as two independent variables for free vibrations of rectangular plate. Mousavi et al. [27] used a variational approach based on Hamilton's principle to develop the governing equations for the dynamic analysis of plates using the Reddy third-order shear deformable plate theory with strain gradient and velocity gradient. Wanget al. [28] presented a unified solution procedure based on the first-order shear deformation theory for the free vibration analysis of moderately thick orthotropic rectangular plates with general boundary restraints, internal line supports and resting on elastic foundation. Zhou and Zhu [29] utilized the third-order shear deformation plate theory to analyze the vibration and bending of the simply-supported magneto-electro-elastic rectangular plates. Babagi et al. [30] solved 3D elasticity equations by use of the displacement potential functions and the exact solution of a simply supported thick rectangular plate under moving load. Javidi et al. [31] considered transverse and longitudinal vibration of nonlinear plate under exacting of orbiting mass based on first order shear deformation theory. Makvandi et al. [32] proposed a hybrid method to investigate the nonlinear vibrations of pre- and post-buckled rectangular plates . Daneshmehr et al. [33] investigated the free vibration behavior of the nanoplate made of functionally graded materials with small-scale effects. The generalized differential quadrature method (GDQM) was used to solve the governing equations for various boundary conditions to obtain the nonlinear natural frequencies of FG nanoplates. Hosseini et al. [34] studied stress distribution in a single-walled carbon nanotube under internal pressure with various chirality. Hosseini et al. [35] presented the stress analysis of ratating nano-disk of functionally graded materials with nonlinearly varying thickness based on strain gradient theory. Zamani Nejad et al. [36] used a semi-analytical iterative method as one of the newest analytical methods for the elastic analysis of thick-walled spherical pressure vessels made of functionally graded materials subjected to internal pressure. In other work, Zamani Nejad and Hadi [37] formulated the problem of the static bending of Euler-Bernoulli nano-beams made of bi-directional functionally graded material with small scale effects. Also, Zamani Nejad and Hadi [38] investigated the free vibration analysis of Euler-Bernoulli nano-beams made of bi-directional functionally graded material with small scale effects. Zamani Nejad et al. [39] presented consistent couple-stress theory for free vibration analysis of Euler-Bernoulli nano-beams made of arbitrary bi-directional functionally graded materials Also, Zamani Nejad et al. [40] presented buckling analysis of the nano-beams made of two-directional functionally graded materials with small scale effects based on nonlocal elasticity theory. In other work, Zamani Nejad et al. [41] presented an exact closed-form analytical solution for elasto-plastic deformations and stresses in a rotating disk made of functionally graded materials in which the elasto-perfectly-plastic material model is employed. Shishesaz et al. [42] studied the thermoelastic behavior of a functionally graded nanodisk based on the strain gradient theory. Hadi et al. [43] presented buckling analysis of FGM Euler-Bernoulli nano-beams with 3D-varying properties based on consistent couple-stress theory. Zamani Nejad et al. [44] discussed some critical issues and problems in the development of thick shells made from functionally graded piezoelectric material. Hadi et al. [45] presented an investigation on the free vibration of three-directional functionally graded material Euler-Bernoulli nano-beam, with small scale effects.

Even though there are some classical analytical and exact solutions of the nonlocal plate theory , in this methods the natural frequencies are obtained by applying the boundary conditions to the general solution of the differential equation. There is an alternative approach, wave propagation method, which considers vibrations as propagating waves traveling in the structures.

Zhang [46] extended the wave propagation approach to coupled frequency analysis of finite cylindrical shells submerged in a dense acoustic medium. Kang et al. [47] presented wave approach for the free vibration analysis of planar circular curved beam system. Natsuki and Endo [48] presented a vibration analysis of single and double walled carbon nanotubes as well as nanotubes embedded in an elastic matrix using wave propagation approach. Lee et al. [49]considered wave motion in thin, uniform, curved beam with constant curvature. Nikkhah Bahrami et al. [50] presented modified wave approach for calculation of natural frequencies and mode shapes in arbitrary non-uniform beams. Bahrami et al[51] analysed the free vibration of annular circular and sectorial membranes using the wave propagation approach. Bahrami and

Teimourian [52] combined the wave propagation approach with nonlocal elasticity theory to analyze the buckling and free vibration of Euler-Bernolli nanobeams. In another work, Bahrami and Teimourian [53] presented the wave propagation approach for free vibration analysis of composite annular and circular membranes. Furthermore, Bahrami and Teimourian [54] developed the wave propagation technique for analyzing the wave power reflection in circular annular nanoplates. Also, the wave propagation approach for free vibration analysis of non-uniform rectangular membranes has been presented by Bahrami and Teimourian [55]. Moreover Bahrami and Teimourian [56] presented the wave approach for analyzing the free vibration and wave reflection in carbon nanotubes. Ilkhani et al. [57] used wave propagation to analysis the free vibration analysis of thin rectangular nanoplates. Recently, Bahrami [58] utilized wave propagation method and differential constitutive law consequent to the Eringen strain-driven integral nonlocal elasticity model to analyze the free vibration, wave-power transmission and reflection in multi-cracked nanorods. Also he utilized wave propagation methods and the nonlocal elasticity theory to analyze the vibration, wave power transmission and reflection in multi-cracked Euler-Bernolli nanobeams [59].

As mentioned in the research literature, the wave propagation method for thick plates has not been used so far. In addition, there were at most two waves in analyzing all the above- mentioned structures while in this study, there are four waves for the first time causing the more complicated problem. In this study, firstly the matrices of propagation and reflection are derived and by combining them, the characteristic equation of the plate is obtained.

2. Modeling and Formulation

In figure 1, isotropic and thick rectangular plate in length a, width b and height h is showed. In Reddy plate theory [3], the displacement components are assume to be given as:

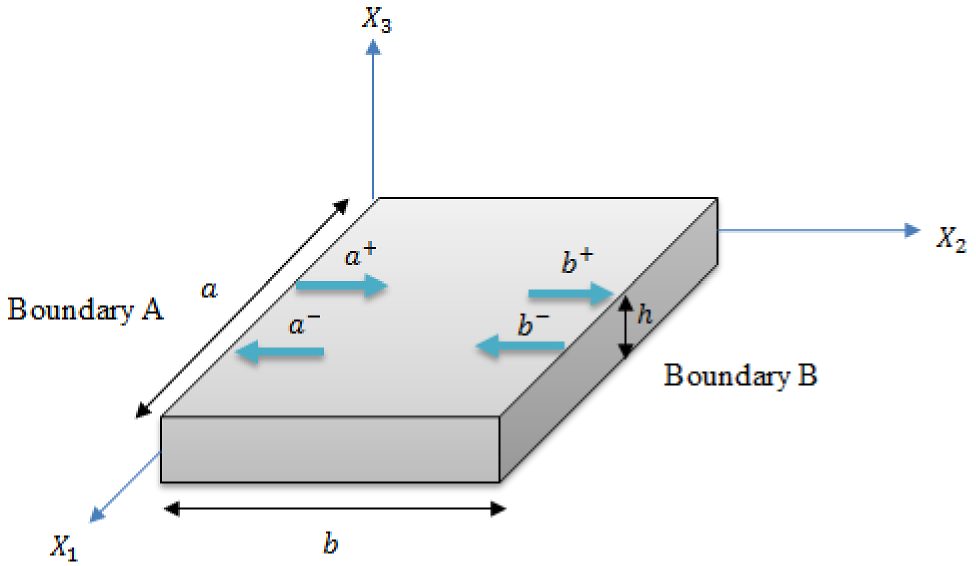

Figure 1. Geometry of rectangular isotropic thick plate

$$u(x_1,x_2,x_3,t)=u_0(x_1,x_2,t)+x_3\varphi_1(x_1,x_2,t)-\frac{4x_3^{\,3}}{3h^2}\left(\varphi_1+\frac{\partial w_0}{\partial x_1}\right) \tag{1a}$$

$$v(x_1,x_2,x_3,t)=v_0(x_1,x_2,t)+x_3\varphi_2(x,y,t)-\frac{4x_3^{\,3}}{3h^2}\left(\varphi_2+\frac{\partial w_0}{\partial x_2}\right) \tag{1b}$$

$$w(x_1,x_2,x_3,t)=w_0(x_1,x_2,t) \tag{1c}$$

where u, v and w are the mid-plane displacements and φ_1, φ_2 respectively shows normal rotation perpendicular to middle of the plate around x_2 and x_1 axes.

By using displacement fields which proposed, strain equation could be written as follows:

$$\varepsilon_{11}=\frac{\partial u_0(x_1,x_2,t)}{\partial x_1}+x_3\frac{\partial\varphi_1(x_1,x_2,t)}{\partial x_1}-\frac{4}{3h^2}x_3^{\,3}\left(\frac{\partial\varphi_1}{\partial x_1}+\frac{\partial^2 w_0}{\partial x_1^{\,2}}\right) \tag{2a}$$

$$\varepsilon_{22}=\frac{\partial v_0(x_1,x_2,t)}{\partial x_2}+x_3\frac{\partial\varphi_2(x_1,x_2,t)}{\partial x_2}-\frac{4}{3h^2}x_3^{\,3}\left(\frac{\partial\varphi_2}{\partial x_2}+\frac{\partial^2 w_0}{\partial x_2^{\,2}}\right) \tag{2b}$$

$$\varepsilon_{33}=0 \tag{2c}$$

$$\varepsilon_{12}=\frac{1}{2}\left(\frac{\partial u_0(x_1,x_2,t)}{\partial x_2}+\frac{\partial v_0(x_1,x_2,t)}{\partial x_1}\right)+x_3\left(\frac{\partial\varphi_1(x_1,x_2,t)}{\partial x_2}+\frac{\partial\varphi_2(x_1,x_2,t)}{\partial x_1}\right)-\frac{4}{3h^2}x_3^{\,3}\left(\frac{\partial\varphi_1}{\partial x_2}+2\times\frac{\partial^2 w_0}{\partial x_1\partial x_2}+\frac{\partial\varphi_2}{\partial x_1}\right) \tag{2d}$$

$$\varepsilon_{13} = \frac{1}{2}(1-\frac{4}{h^2}x_3{}^2)\left(\varphi_1 + \frac{\partial w_0(x_1,x_2,t)}{\partial x_1}\right) \tag{2e}$$

$$\varepsilon_{23} = \frac{1}{2}(1-\frac{4}{h^2}x_3{}^2)\left(\varphi_2 + \frac{\partial w_0(x_1,x_2,t)}{\partial x_2}\right) \tag{2f}$$

So the stress-strain relations for the plane stress problem are defined as:

$$\begin{bmatrix}\sigma_{11}\\ \sigma_{22}\\ \sigma_{12}\\ \sigma_{23}\\ \sigma_{13}\end{bmatrix} = \frac{E}{1-\upsilon^2}\left(\begin{bmatrix} u_{,1}+\upsilon v_{,2}\\ v_{,1}+\upsilon u_{,1}\\ \frac{1-\upsilon}{2}(u_{,2}+v_{,1})\\ \frac{1-\upsilon}{2}(\varphi_2+w_{,2})\\ \frac{1-\upsilon}{2}(\varphi_1+w_{,1})\end{bmatrix} + x_3\begin{bmatrix}\varphi_{1,1}+\upsilon\varphi_{2,2}\\ \varphi_{2,2}+\upsilon\varphi_{1,1}\\ \frac{1-\upsilon}{2}(\varphi_{1,2}+\varphi_{2,1})\\ 0\\ 0\end{bmatrix} - \frac{4x_3^2}{h^2}\begin{bmatrix}0\\ 0\\ 0\\ \frac{1-\upsilon}{2}(\varphi_2+w_{,2})\\ \frac{1-\upsilon}{2}(\varphi_1+w_{,1})\end{bmatrix} - \frac{4x_3^3}{h^2}\begin{bmatrix}(\varphi_{1,1}+w_{,11})+\upsilon(\varphi_{2,2}+w_{,22})\\ (\varphi_{2,2}+w_{,22})+\upsilon(\varphi_{1,1}+w_{,11})\\ \frac{1-\upsilon}{2}(\varphi_{1,2}+\varphi_{2,1}+2w_{,12})\\ 0\\ 0\end{bmatrix}\right) \tag{3}$$

Where E is the Young modulus of elasticity and υ is the Poisson's ratio.

Also, the stress resultants are defined by:

$$(N_i, M_i, P_i) = \int_{\frac{-h}{2}}^{\frac{h}{2}} \sigma_i(1, x_3, x_3^3)dx_3 \quad \text{(i=1,2,6)} \tag{4a}$$

$$(Q_2, R_2) = \int_{\frac{-h}{2}}^{\frac{h}{2}} \sigma_4(1, x_3^2)dx_3 \tag{4b}$$

$$(Q_1, R_1) = \int_{\frac{-h}{2}}^{\frac{h}{2}} \sigma_5(1, x_3^2)dx_3 \tag{4c}$$

$\sigma_{11}=\sigma_1,\ \sigma_{22}=\sigma_2,\ \sigma_{23}=\sigma_4,\ \sigma_{13}=\sigma_5,\ \sigma_{12}=\sigma_6$

The non-dimensional equations of motion based on third-order shear deformation plate theory for a thick rectangular plate are [21]:

$$\begin{aligned}&[\frac{68}{210}(1-\upsilon)\nabla^2\overline{\varphi_1} + \frac{68}{210}(1+\upsilon)(\overline{\varphi_{1.11}} + \overline{\varphi_{2,12}}) - \frac{16}{105}\nabla^2\overline{w_{,1}}\\ &-\frac{16}{5\tau^2}(1-\upsilon)(\overline{\varphi_1}+\overline{w_{,1}})] =\\ &-\frac{17}{315}\tau^2\beta^2\overline{\varphi_1} + \frac{4}{315}\tau^2\beta^2\overline{w_{,1}}\end{aligned} \tag{5a}$$

$$\begin{aligned}&[\frac{68}{210}(1-\upsilon)\nabla^2\overline{\varphi_2} + \frac{68}{210}(1+\upsilon)(\overline{\varphi_{2,22}} + \overline{\varphi_{1,12}}) - \frac{16}{105}\nabla^2\overline{w_{,2}}\\ &-\frac{16}{5\tau^2}(1-\upsilon)(\overline{\varphi_2}+\overline{w_{,2}})] =\\ &-\frac{17}{315}\tau^2\beta^2\overline{\varphi_2} + \frac{4}{315}\tau^2\beta^2\overline{w_{,2}}\end{aligned} \tag{5b}$$

$$\begin{aligned}&\frac{16}{105}\nabla^2(\overline{\varphi_{1,1}}+\overline{\varphi_{2,2}}) - \frac{1}{21}\nabla^4\overline{w} + \frac{16}{5\tau^2}(1-\upsilon)(\overline{\varphi_{1,1}}+\overline{\varphi_{2,2}})\\ &+(\frac{16}{5\tau^2}(1-\upsilon)+N)\nabla^2\overline{w}\\ &= -\beta^2\overline{w} + \frac{1}{252}\tau^2\beta^2\nabla^2\overline{w} - \frac{4}{315}\tau^2\beta^2(\overline{\varphi_{1,1}}+\overline{\varphi_{2,2}})\end{aligned} \tag{5c}$$

A comma followed by 1, 2 or 3 represents the partial derivatives with respect to the normalized coordinates (X_1, X_2, X_3) . $\overline{w}$ is non-dimensional transverse displacement, $\overline{\varphi_1}$ and $\overline{\varphi_2}$ are non-dimensional slope due to bending alone in the respective planes which are defined by the following relations:

$$\overline{\varphi_1}(X_1, X_2, t) = \varphi_1(x_1, x_2)e^{-i\omega t} \tag{6a}$$

$$\overline{\varphi_2}(X_1, X_2, t) = \varphi_2(x_1, x_2)e^{-i\omega t} \tag{6b}$$

$$\overline{w}(X_1, X_2, t) = \frac{w(x_1, x_2)e^{-i\omega t}}{a} \tag{6c}$$

Also the non-dimensional variables thickness to length ratio τ , aspect ratio δ , frequency parameter β , buckling load N and dimensionless coordinates $\bar{X}_1$ and $\bar{X}_2$ are defined as follows:

$$\bar{X}_1 = \frac{x_1}{a},\ \bar{X}_2 = \frac{x_2}{b},\ \tau = \frac{h}{a},\ \delta = \frac{b}{a},\ \beta = \omega a^2\sqrt{\frac{\rho h}{D}},\ N = \frac{a^2}{D}N_{xx} \tag{7}$$

where $D = \dfrac{Eh^3}{12(1-\upsilon^2)}$.

3. Solution method

3.1 Solving by the wave propagation method

Solving the governing equations on the Reddy plate can be obtained by expressing the dimensionless functions $\overline{\varphi_1}$, $\overline{\varphi_2}$ and $\overline{w}$ in the form of the dimensionless functions of potential W_1, W_2, W_3 and W_4 as follows [21]:

$$\overline{\varphi_1} = C_1 W_{1,1} + C_2 W_{2,1} + C_3 W_{3,1} + W_{4,2} \tag{8a}$$

$$\overline{\varphi_2} = C_1 W_{1,2} + C_2 W_{2,2} + C_3 W_{3,2} + W_{4,1} \tag{8b}$$

$$\overline{w} = W_1 + W_2 + W_3 \tag{8c}$$

where

$$C_i = \frac{\dfrac{-16(1-\upsilon)}{5\delta^2} - \dfrac{4\delta^2\beta^2}{315} + \alpha_i^2 \dfrac{16}{105}}{\alpha_i^2 \dfrac{68}{105} + \dfrac{16(1-\upsilon)}{5\delta^2} - \dfrac{17\beta^2\delta^2}{315}} \quad (i = 1,2,3) \tag{9}$$

Based on these considered potential functions, if the plate equations are rewritten, the differential equations will be the so-called decoupled for these functions:

$$\nabla^2 W_1 + \alpha_1^2 W_1 = 0,\ \nabla^2 W_2 + \alpha_2^2 W_2 = 0,\ \nabla^2 W_3 + \alpha_3^2 W_3 = 0 \tag{10}$$

In which α_1^2, α_2^2 and α_3^2 can be obtained by solving the following equation:

$$y^3 + a_1 y^2 + a_2 y + a_3 = 0 \tag{11}$$

where

$$a_1 = \frac{-2520 + 2520\upsilon + \delta^4\beta^2 - 510N\delta^2}{6\delta^2} \tag{12a}$$

$$a_2 = 5\beta^2(-24 + 7\upsilon) + \frac{-1020N\delta^2\beta^2 + \delta^4\beta^4}{144} \tag{12b}$$

$$a_3 = -\frac{5\beta^2\left(-1008 + 1008\upsilon + 17\delta^4\beta^2\right)}{12\delta^2} \tag{12c}$$

Also:

$$\nabla^2 W_4 + \alpha_4^2 W_4 = 0 \tag{13}$$

$$\alpha_4^2 = \frac{17\delta^4\beta^2 - 1008(1-\upsilon)}{102(1-\upsilon)\delta^2} \tag{14}$$

Using the method of separation of variables, an answer set is obtained for equations 10:

$$W_1 = \left[A_1 \sin h(\lambda_1 X_2) + A_2 \cosh(\lambda_1 X_2)\right]\sin(\mu_1 X_1) + \left[B_1 \sin h(\lambda_1 X_2) + B_2 \cos h(\lambda_1 X_2)\right]\cos(\mu_1 X_1) \tag{15a}$$

$$W_2 = \left[A_3 \sinh(\lambda_2 X_2) + A_4 \cosh(\lambda_2 X_2)\right]\sin(\mu_2 X_1) + \left[B_3 \sinh(\lambda_2 X_2) + B_4 \cosh(\lambda_2 X_2)\right]\cos(\mu_2 X_1) \tag{15b}$$

$$W_3 = \left[A_5 \sin(\lambda_3 X_2) + A_6 \cos(\lambda_3 X_2)\right] sin(\mu_3 X_1) + \left[B_5 \sin(\lambda_2 X_2) + B_6 \cos(\lambda_2 X_2)\right] cos(\mu_3 X_1) \tag{15c}$$

$$W_4 = \left[A_7 \sinh(\lambda_4 X_2) + A_8 \cosh(\lambda_4 X_2)\right] cos(\mu_4 X_1) + \left[B_7 \sinh(\lambda_4 X_2) + B_8 \cosh(\lambda_4 X_2)\right] sin(\mu_4 X_1) \tag{15d}$$

In which A_i and B_i are the arbitrary constants and λ_i and μ_i which are the wave numbers in two directions of X_2 and X_1, are depended on α_i:

$$\alpha_1^2 = \mu_1^2 + \lambda_1^2;\ \alpha_2^2 = \mu_2^2 + \lambda_2^2;\ \alpha_3^2 = \mu_3^2 + \lambda_3^2;\ \alpha_4^2 = \mu_4^2 + \lambda_4^2 \tag{16}$$

Based on the third-order shear theory, the boundary conditions for two parallel corners (for example $X_1 = 0$ and $X_1 = 1$) are as follows:

Simply supported:

$$\overline{M_2} = \overline{\varphi_1} = \overline{w} = \overline{P_2} = 0 \tag{17}$$

Clamped

$$\overline{\varphi_1} = \overline{\varphi_2} = \overline{w} = \overline{w_{,2}} = 0 \tag{18}$$

In which:

$$\overline{M_1} = \frac{aM_1}{12D};\ \overline{P_2} = \frac{aP_2}{12h^2 D}; \tag{19}$$

Now, by considering the simply support conditions in the corners $X_1 = 0$ and $X_1 = 1$ and applying our wave answers to these support conditions, answers can be written as follows:

$$\mu_1 = \mu_2 = \mu_3 = m\pi \tag{20}$$

$$W_1 = \left[A_1 \sinh(\lambda_1 X_2) + A_2 \cos h(\lambda_1 X_2)\right]\sin(m\pi X_1) \tag{21a}$$

$$W_2 = \left[A_3 \sinh(\lambda_2 X_2) + A_4 \cosh(\lambda_2 X_2)\right]\sin(m\pi X_1) \tag{21b}$$

$$W_3 = \left[A_5 \sin(\lambda_3 X_2) + A_6 \cos(\lambda_3 X_2)\right] sin(m\pi X_1) \tag{21c}$$

$$W_3 = \left[A_7 \sinh\left(\lambda_4 X_2\right) + A_8 \cosh\left(\lambda_4 X_2\right)\right] cos\left(m\pi X_1\right) \tag{21d}$$

By substituting the formulas W_i in equations related to potential function and considering the following equations, $\overline{\varphi_i}$ and $\overline{w}$ can be obtained:

$$\sin(\theta) = \frac{e^{i\theta} - e^{-i\theta}}{2i};\cos(\theta) = \frac{e^{i\theta} + e^{-i\theta}}{2};$$
$$\sinh(\theta) = \frac{e^{\theta} - e^{-\theta}}{2};\cosh(\theta) = \frac{e^{\theta} + e^{-\theta}}{2} \tag{22}$$

Which we will have:

$$\begin{aligned}\overline{\varphi_1} = [&A_1^{'}C_1 m\pi e^{\lambda_1 X_2} + A_2^{'}C_1 m\pi e^{-\lambda_1 X_2} + A_3^{'}C_2 m\pi e^{\lambda_2 X_2} \\ &+A_4^{'}C_2 m\pi e^{-\lambda_2 X_2} + A_5^{'}C_3 m\pi e^{i\lambda_3 X_2} + A_6^{'}C_3 m\pi e^{-i\lambda_3 X_2} \\ &+A_7^{'}\lambda_4 e^{\lambda_4 X_2} + A_8^{'}\lambda_4 e^{-\lambda_4 X_2})\cos(m\pi X_1)\end{aligned} \tag{23a}$$

$$\begin{aligned}\overline{\varphi_2} = [&A_1^{''}C_1\lambda_1 e^{\lambda_1 X_2} + A_2^{''}C_1\lambda_1 e^{-\lambda_1 X_2} + A_3^{''}C_2\lambda_2 e^{\lambda_2 X_2} \\ &+A_4^{''}C_2\lambda_2 e^{-\lambda_2 X_2} + A_5^{''}C_3\lambda_3 e^{i\lambda_3 X_2} + A_6^{''}C_3\lambda_3 e^{-i\lambda_3 X_2} \\ &+A_7^{''}m\pi e^{\lambda_4 X_2} + A_8^{''}m\pi e^{-\lambda_4 X_2}]\sin(m\pi X_1)\end{aligned} \tag{23b}$$

$$\begin{aligned}\overline{w} = [&A_1^{'''}e^{\lambda_1 X_2} + A_2^{'''}e^{-\lambda_1 X_2} + A_3^{'''}e^{\lambda_2 X_2} + A_4^{'''}e^{-\lambda_2 X_2} \\ &+A_5^{'''}e^{i\lambda_3 X_2} + A_6^{'''}e^{-i\lambda_3 X_2}]\sin(m\pi X_1)\end{aligned} \tag{23c}$$

In which:

$$A_1^{'} = \frac{A_1 + A_2}{2};\ A_2^{'} = \frac{A_2 - A_1}{2};\ A_3^{'} = \frac{A_3 + A_4}{2} \tag{24a}$$

$$A_4^{'} = \frac{A_4 + A_3}{2};\ A_5^{'} = \frac{A_6 - iA_5}{2};\ A_6^{'} = \frac{iA_5 + A_6}{2} \tag{24b}$$

$$A_7^{'} = \frac{A_7 + A_8}{2};\ A_8^{'} = \frac{A_7 - A_8}{2} \tag{24c}$$

As it can be seen, in the equations above, $A_i^{''}$ and $A_i^{'''}$ can be written based on $A_i^{'}$:

$$A_1^{'} = A_1^{''} = A_1^{'''}; A_2^{'} = A_2^{''} = -A_2^{'''}; A_3^{'} = A_3^{''} \tag{25a}$$

$$A_4^{'} = -A_4^{''} = A_4^{'''}; A_5^{'} = -iA_5^{''} = A_5^{'''}; A_6^{'} = iA_6^{''} = -A_6^{'''} \tag{25b}$$

$$A_7^{'''} = A_8^{'''} = 0,; A_7^{'} = A_7^{''}; A_8^{'} = -A_8^{''} \tag{25c}$$

Finally, we will have:

$$\overline{\varphi_1} = \begin{bmatrix} A_1^{'}C_1 m\pi e^{\lambda_1 X_2} + A_2^{'}C_1 m\pi e^{-\lambda_1 X_2} \\ +A_3^{'}C_2 m\pi e^{\lambda_2 X_2} + A_4^{'}C_2 m\pi e^{-\lambda_2 X_2} \\ +A_5^{'}C_3 m\pi e^{i\lambda_3 X_2} + A_6^{'}C_3 m\pi e^{-i\lambda_3 X_2} \\ +A_7^{'}\lambda_4 e^{\lambda_4 X_2} + A_8^{'}\lambda_4 e^{-\lambda_4 X_2} \end{bmatrix} \cos\left(m\pi X_1\right) \tag{26a}$$

$$\overline{\varphi_2} = \begin{bmatrix} A_1^{'}C_1\lambda_1 e^{\lambda_1 X_2} - A_2^{'}C_1\lambda_1 e^{-\lambda_1 X_2} \\ +A_3^{'}C_2\lambda_2 e^{\lambda_2 X_2} - A_4^{'}C_2\lambda_2 e^{-\lambda_2 X_2} \\ +iA_5^{'}C_3\lambda_3 e^{i\lambda_3 X_2} - iA_6^{'}C_3\lambda_3 e^{-i\lambda_3 X_2} \\ +A_7^{'}m\pi e^{\lambda_4 X_2} - A_8^{'}m\pi e^{-\lambda_4 X_2} \end{bmatrix} \sin\left(m\pi X_1\right) \tag{26b}$$

$$\overline{w} = \begin{bmatrix} A_1^{'}e^{\lambda_1 X_2} + A_2^{'}e^{-\lambda_1 X_2} + A_3^{'}e^{\lambda_2 X_2} + A_4^{'}e^{-\lambda_2 X_2} \\ +A_5^{'}e^{i\lambda_3 X_2} + A_6^{'}e^{-i\lambda_3 X_2} \end{bmatrix} \sin\left(m\pi X_1\right) \tag{26c}$$

In above equations, sentences with even indexes show a wave that moves in the positive direction of the dimensionless X_2 axis and sentences with odd indexes show a wave that moves in the negative direction of the X_2 axis.

According to what was said, we can write:

$$a^{+}(x) = \begin{Bmatrix} A_2^{'}e^{-\lambda_1 X_2} \\ A_4^{'}e^{-\lambda_2 X_2} \\ A_6^{'}e^{-i\lambda_3 X_2} \\ A_8^{'}e^{-\lambda_4 X_2} \end{Bmatrix};\quad a^{-}(x) = \begin{Bmatrix} A_1^{'}e^{\lambda_1 X_2} \\ A_3^{'}e^{\lambda_2 X_2} \\ A_5^{'}e^{i\lambda_3 X_2} \\ A_7^{'}e^{\lambda_4 X_2} \end{Bmatrix} \tag{27}$$

*3.2 **Propagation** Matrix*

Consider two points on the plate a distance X^0 apart in X_2 direction as shown in Figure 2. Positive- and negative-going waves propagate from one point to another and they are related to each other using the following equations:

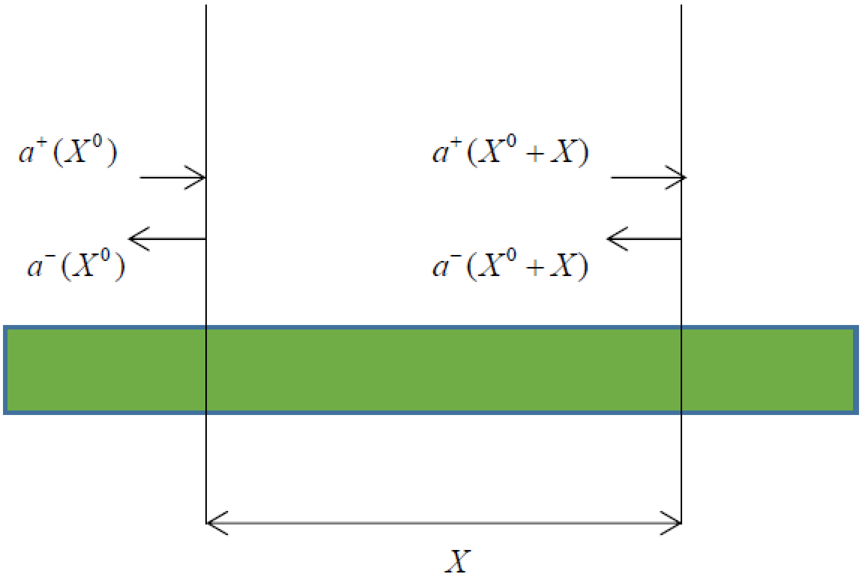

Figure 2 A lateral view of Reddy plate representing positive and negative going propagating waves

$$a^+\left(X+X^0\right)=f^+(X)a^+\left(X^0\right),\ a^-\left(X^0\right)=f^-(X)a^-\left(X+X^0\right) \tag{28}$$

Where $X^0=(X_1^0,X_2^0,X_3^0)$, is an arbitrary point on the plate, $X=(X_1,X_2,X_3)$ is the position of any point relative to X^0 in X_2 direction, and $f^+(X)$ is the propagation matrix in the positive direction and $f^-(X)$ is the propagation matrix in the negative direction. By substituting the wave domain equations in equations above, we will have:

$$f^+(X)=f^-(X)=\begin{bmatrix} e^{-\lambda_1\delta X_2} & 0 & 0 & 0 \\ 0 & e^{-\lambda_2\delta X_2} & 0 & 0 \\ 0 & 0 & e^{-i\lambda_3\delta X_2} & 0 \\ 0 & 0 & 0 & e^{-\lambda_4\delta X_2} \end{bmatrix} \tag{29}$$

As it is seen, the propagation functions in the positive and negative directions are equal to each other and they are called $f(X)$.This is a property which cannot be appeared in non-uniform plates and in them; the propagation matrices are different from each other in the positive and negative directions.

3.3 Reflection Matrix

When the propagated waves in the plate are collided to the boundaries, they are reflected and this action obviously presents that as long as the plate is vibrating, positive and negative waves are propagating in the environment.

Equation between positive and negative travelling waves with the reflection matrix r will be provided:

$$a^-=ra^+ \tag{30}$$

For obtaining the reflection of waves in the boundaries, the boundary conditions will be used. For two boundary modes of simple and clamped, we try to express the reflection of the propagated waves in the plate.

3.4 Reflection matrix for the simply support boundary condition

In this case, the boundary conditions, as previously said, are as follows:

$$\overline{M}_2=\overline{\varphi}_1=\overline{w}=\overline{P}_2=0 \tag{31}$$

The incoming wave to this boundary is called a^+ and the reflected wave from the boundary is called a^-.

$$\begin{aligned}\overline{M}_2=&\left[\frac{1}{60}\pi^4m^2\upsilon-\frac{1}{15}C_1\pi^2m^2\upsilon-\frac{1}{60}\mu_1^2+\frac{1}{15}C_1\mu_1^2\right]a_1^-\\&+\left[\frac{1}{60}\pi^4m^2\upsilon-\frac{1}{15}C_1\pi^2m^2\upsilon-\frac{1}{60}\mu_1^2+\frac{1}{15}C_1\mu_1^2\right]a_1^+\\&+\left[\frac{1}{60}\pi^4m^2\upsilon-\frac{1}{15}C_2\pi^2m^2\upsilon-\frac{1}{60}\mu_2^2+\frac{1}{15}C_2\mu_2^2\right]a_2^-\\&+\left[\frac{1}{60}\pi^4m^2\upsilon-\frac{1}{15}C_2\pi^2m^2\upsilon-\frac{1}{60}\mu_2^2+\frac{1}{15}C_2\mu_2^2\right]a_2^+\\&+\left[\frac{1}{60}\pi^4m^2\upsilon-\frac{1}{15}C_3\pi^2m^2\upsilon-\frac{1}{60}\mu_3^2+\frac{1}{15}C_3\mu_3^2\right]a_3^-\\&+\left[\frac{1}{60}\pi^4m^2\upsilon-\frac{1}{15}C_3\pi^2m^2\upsilon-\frac{1}{60}\mu_3^2+\frac{1}{15}C_3\mu_3^2\right]a_3^+\\&+\left[\frac{1}{60}\pi^4m^2\upsilon-\frac{1}{15}\mu_4m\pi\upsilon+\frac{1}{15}\mu_4m\pi\right]a_4^-\\&+\left[\frac{1}{60}\pi^4m^2\upsilon-\frac{1}{15}\mu_4m\pi\upsilon+\frac{1}{15}\mu_4m\pi\right]a_4^+\end{aligned} \tag{32a}$$

$$\overline{\varphi_1} = \begin{bmatrix} C_1 m\pi a_1^- + C_1 m\pi a_1^+ + C_2 m\pi a_2^- + C_2 m\pi a_2^+ \\ + C_3 m\pi a_3^- + C_3 m\pi a_3^+ + \lambda_4 a_4^- + \lambda_4 a_4^+ \end{bmatrix} = 0 \tag{32b}$$

$$\overline{w} = \left[a_1^- + a_1^+ + a_2^- + a_2^+ + a_3^- + a_3^+ \right] = 0 \tag{32c}$$

$$\begin{aligned} \overline{P_2} = &\left[\frac{1}{336}\pi^2 m^2 \upsilon - \frac{1}{105} C_1 \pi^2 m^2 \upsilon + \frac{1}{105} C_1 \mu_1^2 - \frac{1}{336}\mu_1^2 \right] a_1^- \\ &+ \left[\frac{1}{336}\pi^2 m^2 \upsilon - \frac{1}{105} C_1 \pi^2 m^2 \upsilon + \frac{1}{105} C_1 \mu_1^2 - \frac{1}{336}\mu_1^2 \right] a_1^+ \\ &+ \left[\frac{1}{336}\pi^2 m^2 \upsilon - \frac{1}{105} C_2 \pi^2 m^2 \upsilon + \frac{1}{105} C_2 \mu_2^2 - \frac{1}{336}\mu_2^2 \right] a_2^- \\ &+ \left[\frac{1}{336}\pi^2 m^2 \upsilon - \frac{1}{105} C_2 \pi^2 m^2 \upsilon + \frac{1}{105} C_2 \mu_2^2 - \frac{1}{336}\mu_2^2 \right] a_2^+ \\ &+ \left[\frac{1}{336}\pi^2 m^2 \upsilon - \frac{1}{105} C_3 \pi^2 m^2 \upsilon + \frac{1}{105} C_3 \mu_3^2 - \frac{1}{336}\mu_3^2 \right] a_3^- \\ &+ \left[\frac{1}{336}\pi^2 m^2 \upsilon - \frac{1}{105} C_3 \pi^2 m^2 \upsilon + \frac{1}{105} C_3 \mu_3^2 - \frac{1}{336}\mu_3^2 \right] a_3^+ \\ &+ \left[-\frac{1}{105}\mu_4 m\pi\upsilon + \frac{1}{105}\mu_4 m\pi \right] a_4^- \\ &+ \left[-\frac{1}{105}\mu_4 m\pi\upsilon + \frac{1}{105}\mu_4 m\pi \right] a_4^+ \end{aligned} \tag{32d}$$

That by writing it in the form of matrix, the reflection matrix for the simply supported mode is:

$$r_s = A^{-1} B \tag{33}$$

$$r_s = -\begin{bmatrix} A_{11} & A_{12} & A_{13} & A_{14} \\ C_1 m\pi & C_2 m\pi & C_3 m\pi & \lambda_4 \\ 1 & 1 & 1 & 0 \\ A_{41} & A_{42} & A_{43} & A_{44} \end{bmatrix}^{-1} \times \begin{bmatrix} B_{11} & B_{12} & B_{13} & B_{14} \\ C_1 m\pi & C_2 m\pi & C_3 m\pi & \lambda_4 \\ 1 & 1 & 1 & 0 \\ B_{41} & B_{42} & B_{43} & B_{44} \end{bmatrix} \tag{34}$$

In which:

$$A_{11} = B_{11} = \left[\frac{1}{60}\pi^4 m^2 \upsilon - \frac{1}{15} C_1 \pi^2 m^2 \upsilon - \frac{1}{60}\mu_1^2 + \frac{1}{15} C_1 \mu_1^2 \right] \tag{35a}$$

$$A_{12} = B_{12} = \left[\frac{1}{60}\pi^4 m^2 \upsilon - \frac{1}{15} C_2 \pi^2 m^2 \upsilon - \frac{1}{60}\mu_2^2 + \frac{1}{15} C_2 \mu_2^2 \right] \tag{35b}$$

$$A_{13} = B_{14} = \left[\frac{1}{60}\pi^4 m^2 \upsilon - \frac{1}{15} C_3 \pi^2 m^2 \upsilon - \frac{1}{60}\mu_3^2 + \frac{1}{15} C_3 \mu_3^2 \right] \tag{35c}$$

$$A_{14} = B_{14} = \left[\frac{1}{60}\pi^4 m^2 \upsilon - \frac{1}{15}\mu_4 m\pi\upsilon + \frac{1}{15}\mu_4 m\pi \right] \tag{35d}$$

$$A_{41} = B_{41} = \left[\frac{1}{336}\pi^2 m^2 \upsilon - \frac{1}{105} C_1 \pi^2 m^2 \upsilon + \frac{1}{105} C_1 \mu_1^2 - \frac{1}{336}\mu_1^2 \right] \tag{35e}$$

$$A_{42} = B_{42} = \left[\frac{1}{336}\pi^2 m^2 \upsilon - \frac{1}{105} C_2 \pi^2 m^2 \upsilon + \frac{1}{105} C_2 \mu_2^2 - \frac{1}{336}\mu_2^2 \right] \tag{35f}$$

$$A_{43} = B_{43} = \left[\frac{1}{336}\pi^2 m^2 \upsilon - \frac{1}{105} C_3 \pi^2 m^2 \upsilon + \frac{1}{105} C_3 \mu_3^2 - \frac{1}{336}\mu_3^2 \right] \tag{35g}$$

$$A_{44} = B_{44} = \left[-\frac{1}{105}\mu_4 m\pi\upsilon + \frac{1}{105}\mu_4 m\pi \right] \tag{35h}$$

In this case, this matrix will be a negative identity matrix, that is:

$$r_s = -I \tag{36}$$

3.5 Reflection matrix for the Clamped boundary condition

In the clamped mode, the boundary condition is as follows:

$$\overline{\varphi_1} = \overline{\varphi_2} = \overline{w} = \overline{w_{,2}} = 0 \tag{37}$$

$$\overline{\varphi_1} = \begin{bmatrix} C_1 m\pi a_1^- + C_1 m\pi a_1^+ + C_2 m\pi a_2^- + C_2 m\pi a_2^+ \\ + C_3 m\pi a_3^- + C_3 m\pi a_3^+ + \lambda_4 a_4^- + \lambda_4 a_4^+ \end{bmatrix} = 0 \tag{38a}$$

$$\overline{\varphi_2} = \begin{bmatrix} C_1 \lambda_1 a_1^- - C_1 \lambda_1 a_1^+ + C_2 \lambda_2 a_2^- - C_2 \lambda_2 a_2^+ \\ + iC_3 \lambda_3 a_3^- - iC_3 \lambda_3 a_3^+ + m\pi a_4^- - m\pi a_4^+ \end{bmatrix} = 0 \tag{38b}$$

$$\overline{w} = [a_1^- + a_1^+ + a_2^- + a_2^+ + a_3^- + a_3^+] = 0 \tag{38c}$$

$$\overline{w_{,2}} = \left[\lambda_1 a_1^- - \lambda_1 a_1^+ + \lambda_2 a_2^- - \lambda_2 a_2^+ + i\,\lambda_3 a_3^- - i\,\lambda_3 a_3^+ \right] = 0 \tag{38d}$$

Therefore, the reflection matrix for the clamped mode is as follows:

$$r_C = -\begin{bmatrix} 1 & 1 & 1 & 0 \\ C_1 m\pi & C_2 m\pi & C_3 m\pi & \lambda_4 \\ C_1 \lambda_1 & C_2 \lambda_2 & C_3 i\,\lambda_3 & m\pi \\ \lambda_1 & \lambda_2 & i\,\lambda_3 & 0 \end{bmatrix}^{-1} \times \begin{bmatrix} 1 & 1 & 1 & 0 \\ C_1 m\pi & C_2 m\pi & C_3 m\pi & \lambda_4 \\ -C_1 \lambda_1 & -C_2 \lambda_2 & -C_3 i\,\lambda_3 & -m\pi \\ -\lambda_1 & -\lambda_2 & -i\,\lambda_3 & 0 \end{bmatrix} \tag{39}$$

3.6 Analyzing the free vibrations of the Reddy plate

Consider the plate shown in Figure 1. For analyzing this plate using our wave method, two wave domains for the positive travelling wave and two wave domains for the negative travelling wave in the direction of X_2 at two beginning and ending points are considered. These waves can be related to each other using the obtained propagation and reflection matrices.

$$b^+ = f\left(b\right)a^+; a^- = f\left(b\right)b^- \tag{40}$$

In which $f\left(b\right)$ is the propagation matrix of the wave between two points of A and B in X_2 direction. Also, using the propagation and reflection equations at the boundaries, we will have:

$$a^+ = r_A a^-;\ b^- = r_B b^+ \tag{41}$$

In which r_A and r_B are the reflection matrices at the boundaries A and B, respectively.

By writing equations in the form of matrix, we have:

$$\begin{bmatrix} -I & r_A & 0 & 0 \\ f\left(b\right) & 0 & -I & 0 \\ 0 & -I & 0 & f\left(b\right) \\ 0 & 0 & r_B & -I \end{bmatrix}\begin{bmatrix} a^+ \\ a^- \\ b^+ \\ b^- \end{bmatrix} = 0 \tag{42}$$

And for having determinant answer, this matrix must be zero. By equalizing the determinant of this matrix to zero, the frequency and critical buckling load characteristic equation of the system will be obtained.

4. Results and Discussion

For the validation of the results, the values obtained from the wave propagation method and the results obtained from the research literature are compared. Here, the letters S and C representing the simply supported and clamped boundary conditions. For example, in the SCSC boundary condition, the edges along x = 0 and x = a are simply supported boundary conditions and the edges along y = 0 and y = b are clamped boundary conditions. The values of m and n represented the vibrational modes has m and n half-wave in x and y directions, respectively. For all modes, the Poisson coefficient υ is assumed to be 0.3.

The procedure for obtaining the plate frequencies is specified by the wave propagation method shown in Figure 3. The plot of the real and imaginary part changes of the determinants of equation (42) in terms of the dimensionless frequency for the SCSC boundary condition and assuming m = 1, $\delta = 1$, and $\tau = 0.1$ is shown in Figure 3. As shown in the figure, the intersection of the real and imaginary curves of the determinant with the zero axis represents the root of the determinant and hence the frequency of the plate. Furthermore, on the left of the frequency there is another root which is the cut-off frequency in which there is no sign change in the real and imaginary curves. In Table 1, the dimensionless frequencies of the wave method with reference results [21] for simply supported boundary condition, $\delta = 1, 2$ and $\tau = 0.01, 0.1, 0.2$ are compared and the obtained values indicate the high accuracy of the wave propagation method. In Tables 2-4, the dimensionless frequency values for the first eight modes for boundary conditions of SSSS, SCSS and SCSC are listed for different values of aspect ratio and thickness ratio. The values $\delta = 0.4, 0.5, 1, 1.5, 2$ and $\tau = 0.01, 0.05, 0.1, 0.2$ are assumed.

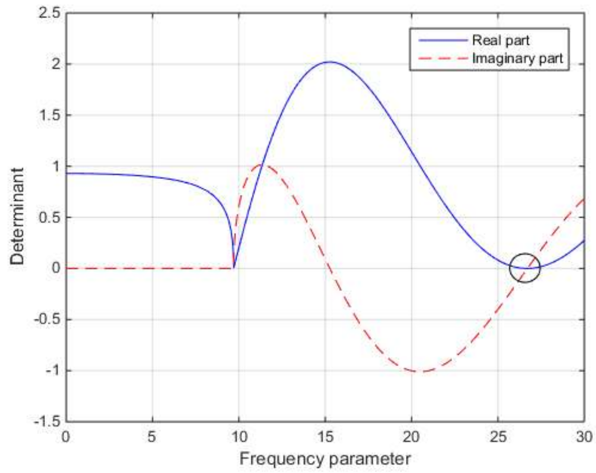

Figure 3 Real and imaginary parts of determinant of Eq. (42) (N=0)

Table 1 Comparison of dimensionless frequency $\beta = \omega a^2 \sqrt{\dfrac{\rho h}{D}}$ for simply supported plates

Method	Aspect ratio	Thickness to length ratio		
		$\tau = 0.01$	$\tau = 0.1$	$\tau = 0.2$
	$\delta = 1$			
Present		**19.7320**	**19.0653**	**17.4523**
[21]		19.7320	19.0653	17.4523
	$\delta = 2$			
Present		**12.3342**	**12.0675**	**11.3717**
[21]		12.3342	12.0675	11.3717

Table 2 *Lowest eight dimensionless frequency parameters* $\beta = \omega a^2 \sqrt{\dfrac{\rho h}{D}}$ *for SSSS plates*

$\delta = \dfrac{b}{a}$	$\tau = \dfrac{h}{a}$	**Frequency parameter**							
		ω_{11}	ω_{21}	ω_{31}	ω_{41}	ω_{12}	ω_{22}	ω_{51}	ω_{32}
0.4	0.01	71.4604	100.9753	150.0956	218.7155	255.4053	284.7216	306.6882	333.5124
		ω_{11}	ω_{21}	ω_{31}	ω_{41}	ω_{12}	ω_{22}	ω_{51}	ω_{32}
	0.05	69.3278	96.8135	141.2294	200.7719	231.5268	255.6034	273.3691	294.7583
		ω_{11}	ω_{21}	ω_{31}	ω_{41}	ω_{12}	ω_{22}	ω_{51}	ω_{32}
	0.1	63.9008	86.9235	122.1579	166.4421	188.2748	204.9556	217.0564	231.4113
		ω_{11}	ω_{21}	ω_{31}	ω_{41}	ω_{12}	ω_{22}	ω_{51}	ω_{32}
	0.2	51.2389	66.5123	88.3739	114.1982	126.4827	135.7246	142.3645	150.1816
		ω_{11}	ω_{21}	ω_{31}	ω_{12}	ω_{22}	ω_{41}	ω_{32}	ω_{51}
0.5	0.01	49.3032	78.8421	128.0024	167.2668	196.6780	196.6780	245.6262	284.7216
		ω_{11}	ω_{21}	ω_{31}	ω_{12}	ω_{22}	ω_{41}	ω_{32}	ω_{51}
	0.05	48.2699	76.2612	121.4491	156.3907	181.9487	181.9487	223.3988	255.6034
		ω_{11}	ω_{21}	ω_{31}	ω_{12}	ω_{22}	ω_{41}	ω_{32}	ω_{51}

	0.1	45.4869	69.8093	106.7350	133.7198	152.7532	152.7532	182.5649	204.9556
		ω_{11}	ω_{21}	ω_{31}	ω_{12}	ω_{22}	ω_{41}	ω_{32}	ω_{51}
	0.2	38.1883	55.2543	78.9865	95.2602	106.3633	106.3633	123.2923	135.7246
		ω_{11}	ω_{12}	ω_{21}	ω_{22}	ω_{13}	ω_{31}	ω_{23}	ω_{32}
1	0.01	19.7320	49.3032	49.3032	78.8421	98.5169	98.5169	128.0024	128.0024
		ω_{11}	ω_{12}	ω_{21}	ω_{22}	ω_{13}	ω_{31}	ω_{23}	ω_{32}
	0.05	19.5625	48.2699	48.2699	76.2612	94.5479	94.5479	121.4491	121.4491
		ω_{11}	ω_{12}	ω_{21}	ω_{22}	ω_{13}	ω_{31}	ω_{23}	ω_{32}
	0.1	19.0653	45.4869	45.4869	69.8093	85.0646	85.0646	106.7350	106.7350
		ω_{11}	ω_{12}	ω_{21}	ω_{22}	ω_{13}	ω_{31}	ω_{23}	ω_{32}
	0.2	17.4523	38.1883	38.1883	55.2543	65.3135	65.3135	78.9865	78.9865
		ω_{11}	ω_{12}	ω_{21}	ω_{13}	ω_{22}	ω_{23}	ω_{14}	ω_{31}
1.5	0.01	14.2523	27.4017	43.8295	49.3032	56.9645	78.8421	79.9355	93.0531
		ω_{11}	ω_{12}	ω_{21}	ω_{13}	ω_{22}	ω_{23}	ω_{14}	ω_{31}
	0.05	14.1635	27.0768	43.0093	48.2699	55.5937	76.2612	77.2848	89.4973
		ω_{11}	ω_{12}	ω_{21}	ω_{13}	ω_{22}	ω_{23}	ω_{14}	ω_{31}
	0.1	13.8984	26.1459	40.7671	45.4869	51.9753	69.8093	70.6756	80.8967
		ω_{11}	ω_{12}	ω_{21}	ω_{13}	ω_{22}	ω_{23}	ω_{14}	ω_{31}
	0.2	12.9938	23.3125	34.6865	38.1883	42.8899	55.2543	55.8370	62.6055
		ω_{11}	ω_{12}	ω_{13}	ω_{21}	ω_{14}	ω_{22}	ω_{23}	ω_{15}
2	0.01	12.3342	19.7320	32.0572	41.9134	49.3032	49.3032	61.6149	71.4604
		ω_{11}	ω_{12}	ω_{13}	ω_{21}	ω_{14}	ω_{22}	ω_{23}	ω_{15}
	0.05	12.2675	19.5625	31.6142	41.1622	48.2699	48.2699	60.0171	69.3278
		ω_{11}	ω_{12}	ω_{13}	ω_{21}	ω_{14}	ω_{22}	ω_{23}	ω_{15}
	0.1	12.0675	19.0653	30.3623	39.0977	45.4869	45.4869	55.8497	63.9008
		ω_{11}	ω_{12}	ω_{13}	ω_{21}	ω_{14}	ω_{22}	ω_{23}	ω_{15}
	0.2	11.3717	17.4523	26.6838	33.4301	38.1883	38.1883	45.6412	51.2389

Table 3 Lowest eight dimensionless frequency parameters $\beta = \omega a^2 \sqrt{\frac{\rho h}{D}}$ for SCSS plates

$\delta = \frac{b}{a}$	$\tau = \frac{h}{a}$	Frequency parameter							
		ω_{11}	ω_{21}	ω_{31}	ω_{41}	ω_{12}	ω_{51}	ω_{22}	ω_{32}
0.4	0.01	103.6226	127.9081	171.6779	236.0340	318.3775	320.8481	343.9528	387.6074
		ω_{11}	ω_{21}	ω_{31}	ω_{41}	ω_{12}	ω_{51}	ω_{22}	ω_{32}
	0.05	97.2819	119.0858	157.7544	212.8085	274.7516	282.1870	294.6811	328.3086
		ω_{11}	ω_{21}	ω_{31}	ω_{41}	ω_{12}	ω_{51}	ω_{22}	ω_{32}
	0.1	83.7062	101.3013	131.6061	172.5332	209.2553	221.0698	223.0865	246.0851
		ω_{11}	ω_{21}	ω_{31}	ω_{41}	ω_{12}	ω_{22}	ω_{51}	ω_{32}
	0.2	60.0741	72.2825	91.8844	116.4351	133.2295	141.7247	143.9137	155.3443
		ω_{11}	ω_{21}	ω_{31}	ω_{41}	ω_{12}	ω_{22}	ω_{32}	ω_{51}
0.5	0.01	69.1918	94.3539	139.7691	205.8254	207.3693	233.3158	277.9118	292.0768
		ω_{11}	ω_{21}	ω_{31}	ω_{12}	ω_{41}	ω_{22}	ω_{32}	ω_{51}
	0.05	66.2898	89.6072	130.7921	187.2540	188.5226	208.9296	245.6071	260.3273
		ω_{11}	ω_{21}	ω_{31}	ω_{12}	ω_{41}	ω_{22}	ω_{32}	ω_{51}
	0.1	59.4159	79.0782	112.3944	151.2530	156.2303	167.1402	193.4631	207.1773
		ω_{11}	ω_{21}	ω_{31}	ω_{12}	ω_{41}	ω_{22}	ω_{32}	ω_{51}
	0.2	45.3311	59.3203	81.1868	101.3727	107.6602	111.3032	127.1003	136.5803
		ω_{11}	ω_{21}	ω_{12}	ω_{22}	ω_{31}	ω_{13}	ω_{32}	ω_{23}
1	0.01	23.6732	51.6188	58.5656	85.9724	100.0773	112.9469	133.4312	140.4237
		ω_{11}	ω_{21}	ω_{12}	ω_{22}	ω_{31}	ω_{13}	ω_{32}	ω_{23}
	0.05	23.3076	50.3745	56.7682	82.4728	95.8532	106.9033	125.8174	131.5798
		ω_{11}	ω_{21}	ω_{12}	ω_{22}	ω_{31}	ω_{13}	ω_{32}	ω_{23}
	0.1	22.4018	47.1306	52.2324	74.2252	85.9319	93.4993	109.4369	113.0723

		ω_{11}	ω_{21}	ω_{12}	ω_{22}	ω_{31}	ω_{13}	ω_{32}	ω_{23}
	0.2	19.7695	39.0576	41.7851	57.2458	65.6858	68.8208	80.0584	81.4198
		ω_{11}	ω_{12}	ω_{21}	ω_{13}	ω_{22}	ω_{23}	ω_{14}	ω_{31}
1.5	0.01	15.5729	31.0506	44.5262	55.3259	59.3913	83.4628	88.2736	93.5123
		ω_{11}	ω_{12}	ω_{21}	ω_{13}	ω_{22}	ω_{23}	ω_{14}	ω_{31}
	0.05	15.4458	30.5479	43.6495	53.8170	57.7814	80.3014	84.6423	89.8856
		ω_{11}	ω_{12}	ω_{21}	ω_{13}	ω_{22}	ω_{23}	ω_{14}	ω_{31}
	0.1	15.0763	29.1608	41.2802	49.9276	53.6518	72.7034	76.0165	81.1602
		ω_{11}	ω_{12}	ω_{21}	ω_{13}	ω_{22}	ω_{23}	ω_{14}	ω_{31}
	0.2	13.8836	25.2698	34.9719	40.5874	43.7450	56.5721	58.2553	62.7217
		ω_{11}	ω_{12}	ω_{13}	ω_{21}	ω_{22}	ω_{14}	ω_{23}	ω_{15}
2	0.01	12.9151	21.5235	35.1847	42.2061	50.3817	53.7626	63.7859	77.2273
		ω_{11}	ω_{12}	ω_{13}	ω_{21}	ω_{22}	ω_{14}	ω_{23}	ω_{15}
	0.05	12.8339	21.2891	34.5732	41.4323	49.2546	52.3853	61.9650	74.4871
		ω_{11}	ω_{12}	ω_{13}	ω_{21}	ω_{22}	ω_{14}	ω_{23}	ω_{15}
	0.1	12.5937	20.6182	32.8950	39.3163	46.2637	48.7954	57.3253	67.7608
		ω_{11}	ω_{12}	ω_{13}	ω_{21}	ω_{22}	ω_{14}	ω_{23}	ω_{15}
	0.2	11.7827	18.5563	28.2680	33.5542	38.6067	39.9877	46.3779	53.0713

Table 4 Lowest eight dimensionless frequency parameters $\beta = \omega a^2 \sqrt{\dfrac{\rho h}{D}}$ for SCSC plates

$\delta = \dfrac{b}{a}$	$\tau = \dfrac{h}{a}$	**Frequency parameter**							
		ω_{11}	ω_{21}	ω_{31}	ω_{41}	ω_{51}	ω_{12}	ω_{22}	ω_{61}
0.4	0.01	144.7717	163.8493	201.0120	259.3302	339.4300	388.6136	410.9773	440.7468
		ω_{11}	ω_{21}	ω_{31}	ω_{41}	ω_{51}	ω_{12}	ω_{22}	ω_{32}
	0.05	130.7472	146.8934	178.7189	227.8760	292.9350	318.2775	334.8247	363.5547
		ω_{11}	ω_{21}	ω_{31}	ω_{41}	ω_{51}	ω_{12}	ω_{22}	ω_{32}
	0.1	105.3502	117.7534	142.6176	179.5712	225.3752	225.6223	240.2965	260.5428
		ω_{11}	ω_{21}	ω_{31}	ω_{41}	ω_{12}	ω_{22}	ω_{51}	ω_{32}
	0.2	70.0180	78.8500	95.8596	118.9387	138.8388	145.6298	147.1191	160.3138
		ω_{11}	ω_{21}	ω_{31}	ω_{41}	ω_{12}	ω_{22}	ω_{51}	ω_{32}
0.5	0.01	94.9541	115.3791	155.945	217.8517	252.3445	275.2150	301.4192	315.4627
		ω_{11}	ω_{21}	ω_{31}	ω_{41}	ω_{12}	ω_{22}	ω_{51}	ω_{32}
	0.05	88.5692	106.8335	142.7990	196.7024	219.3453	237.6635	265.9939	269.7594
		ω_{11}	ω_{21}	ω_{31}	ω_{41}	ω_{12}	ω_{22}	ω_{32}	ω_{51}
	0.1	75.2832	90.1355	119.1323	160.2618	167.8807	181.3243	204.5840	209.6822
		ω_{11}	ω_{21}	ω_{31}	ω_{12}	ω_{41}	ω_{22}	ω_{32}	ω_{51}
	0.2	53.1087	63.8945	83.6539	106.7070	109.0941	115.9685	130.9090	137.5151
		ω_{11}	ω_{21}	ω_{12}	ω_{22}	ω_{31}	ω_{13}	ω_{32}	ω_{23}
1	0.01	28.9241	54.6722	69.1918	94.3539	102.0049	128.6779	139.7691	154.1991
		ω_{11}	ω_{21}	ω_{12}	ω_{22}	ω_{31}	ω_{13}	ω_{32}	ω_{23}
	0.05	28.3174	53.0989	66.2898	89.6072	97.4311	119.9617	130.7921	142.4865
		ω_{11}	ω_{21}	ω_{12}	ω_{22}	ω_{31}	ω_{13}	ω_{32}	ω_{23}
	0.1	26.7084	49.1756	59.4159	79.0783	56.9397	101.9652	112.3944	119.5989
		ω_{11}	ω_{21}	ω_{12}	ω_{22}	ω_{31}	ω_{13}	ω_{32}	ω_{23}
	0.2	22.5355	40.0654	45.3350	59.3313	66.0079	72.2236	80.9208	83.2640

		ω_{11}	ω_{12}	ω_{21}	ω_{13}	ω_{22}	ω_{23}	ω_{31}	ω_{14}
1.5	0.01	17.3647	35.3113	45.3875	61.9589	62.2267	88.6257	94.0450	97.2023
		ω_{11}	ω_{12}	ω_{21}	ω_{13}	ω_{22}	ω_{23}	ω_{31}	ω_{14}
	0.05	17.1727	34.5555	44.4324	59.8339	60.3053	84.7471	90.3301	92.3748
		ω_{11}	ω_{12}	ω_{21}	ω_{13}	ω_{22}	ω_{23}	ω_{14}	ω_{31}
	0.1	16.6309	32.5457	41.8923	54.5868	55.5345	75.7958	81.4351	81.4543
		ω_{11}	ω_{12}	ω_{21}	ω_{13}	ω_{22}	ω_{23}	ω_{14}	ω_{31}
	0.2	14.9956	27.3401	35.2962	42.9797	44.6634	57.9292	60.6219	62.8469
		ω_{11}	ω_{12}	ω_{13}	ω_{21}	ω_{22}	ω_{14}	ω_{23}	ω_{15}
2	0.01	13.6813	23.6321	38.6576	42.5517	51.6188	58.5656	66.2051	83.3313
		ω_{11}	ω_{12}	ω_{13}	ω_{21}	ω_{22}	ω_{14}	ω_{23}	ω_{15}
	0.05	13.5772	23.3076	37.8292	41.7487	50.3746	56.7682	64.1137	79.8770
		ω_{11}	ω_{12}	ω_{13}	ω_{21}	ω_{22}	ω_{14}	ω_{23}	ω_{15}
	0.1	13.2747	22.4018	35.6216	39.5680	47.1306	52.2324	58.9199	71.6869
		ω_{11}	ω_{12}	ω_{13}	ω_{21}	ω_{22}	ω_{14}	ω_{23}	ω_{15}
	0.2	12.2939	19.7696	29.8997	33.6918	39.0577	41.7851	47.1485	54.8783

Figure 4 illustrates the plot of dimensionless frequency changes based on thickness ratio for different values of δ for the three boundary conditions of SSSS, SCSS and SCSC. Regarding the figures, for a constant value of τ, the frequency ratio decreases with increasing the aspect ratio. In addition, by increasing the thickness ratio, the dimensionless frequency values for different values of δ reduce, while the frequency reduction rate is low for larger values of δ. Figure 5 shows the plot of dimensionless frequency changes based on the thickness ratio for the three boundary conditions of SSSS, SCSS, SCSC and $\delta = 1$. As can be observed, the SCSC boundary condition has the highest and SSSS has the e lowest frequency values. Also, it is clear that for SCSC boundary condition, the frequency reduction rate will be higher. The plots of dimensionless frequency changes based on thickness ratio for the first four modes of the above boundary conditions and $\delta = 0.4$ are drawn in Figure 6. It is observed that for higher modes, the frequency reduction rate will be higher. The method for obtaining the critical buckling load is the same as for the method of obtaining a non-dimensional frequency, with the difference that the real and imaginary part of the determinant are plotted in terms of different values of dimensionless critical buckling load N and for $\beta = 0$ (As shown in Figure 7).

Figures 8 illustrate the plot of dimensionless critical buckling load changes based on thickness ratio for different values of δ for the three boundary conditions of SSSS, SCSS and SCSC. The dimensionless buckling load decreases by increasing aspect ratio for a constant value of τ. In addition, by increasing in the thickness ratio, the dimensionless buckling load value for different values of δ reduces. The buckling load reduction rate is low for larger values of δ.

As shown in Figure 9, the SCSC boundary condition has the highest and SSSS has the lowest critical load values. Also, for SCSC boundary condition, the buckling load reduction rate will be higher. In order to verify the critical load obtained from the wave propagation method, in Table 5, the critical load values of the boundary conditions for simply supported boundary condition, $\delta = 1,2$ and $\tau = 0.01, 0.1, 0.2$ are compared with the results obtained from [20]. As is clear, the values obtained by the present method are highly close to the results [20]. In Table 6, the critical loads of the first mode for the three boundary conditions of SSSS, SCSS and SCSC are listed for different values of aspect ratio and thickness ratio, which are assumed to be $\delta = 0.4, 0.5, 1, 1.5, 2$ and $\tau = 0.01, 0.05, 0.1, 0.2$

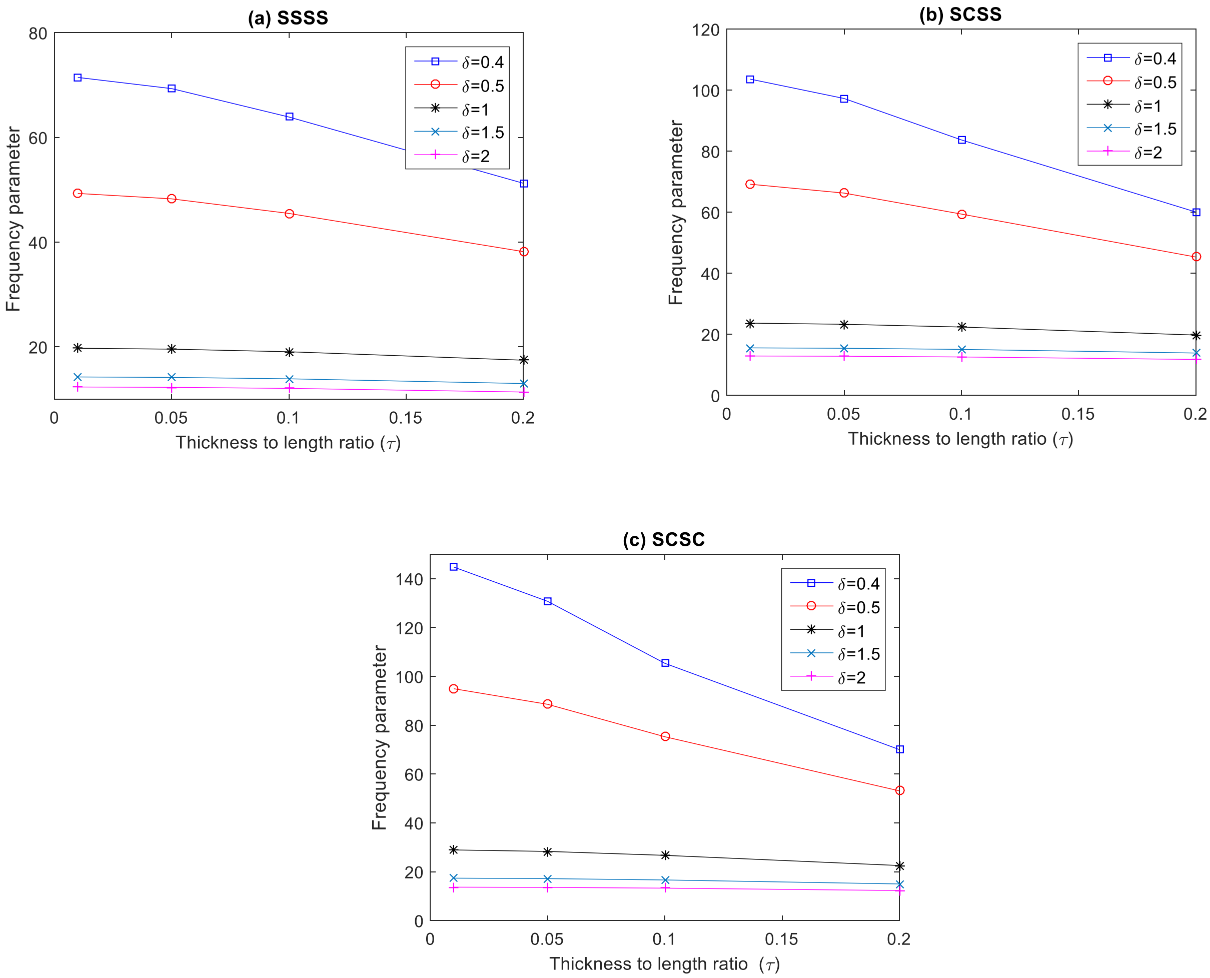

Figure 4 Variations of frequency parameter with thickness to length ratio for various aspect ratios

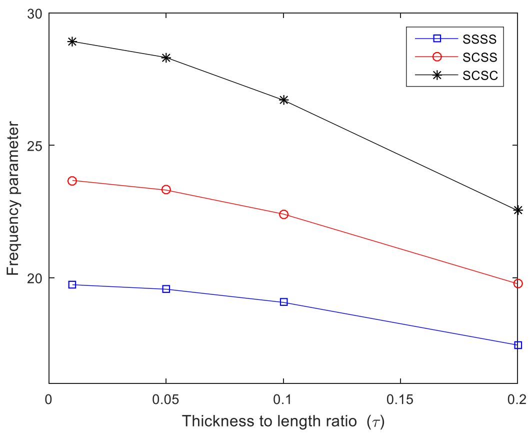

Figure 5 Variations of frequency ratio with thickness to length ratio for various boundary conditions ($\delta = 1$)

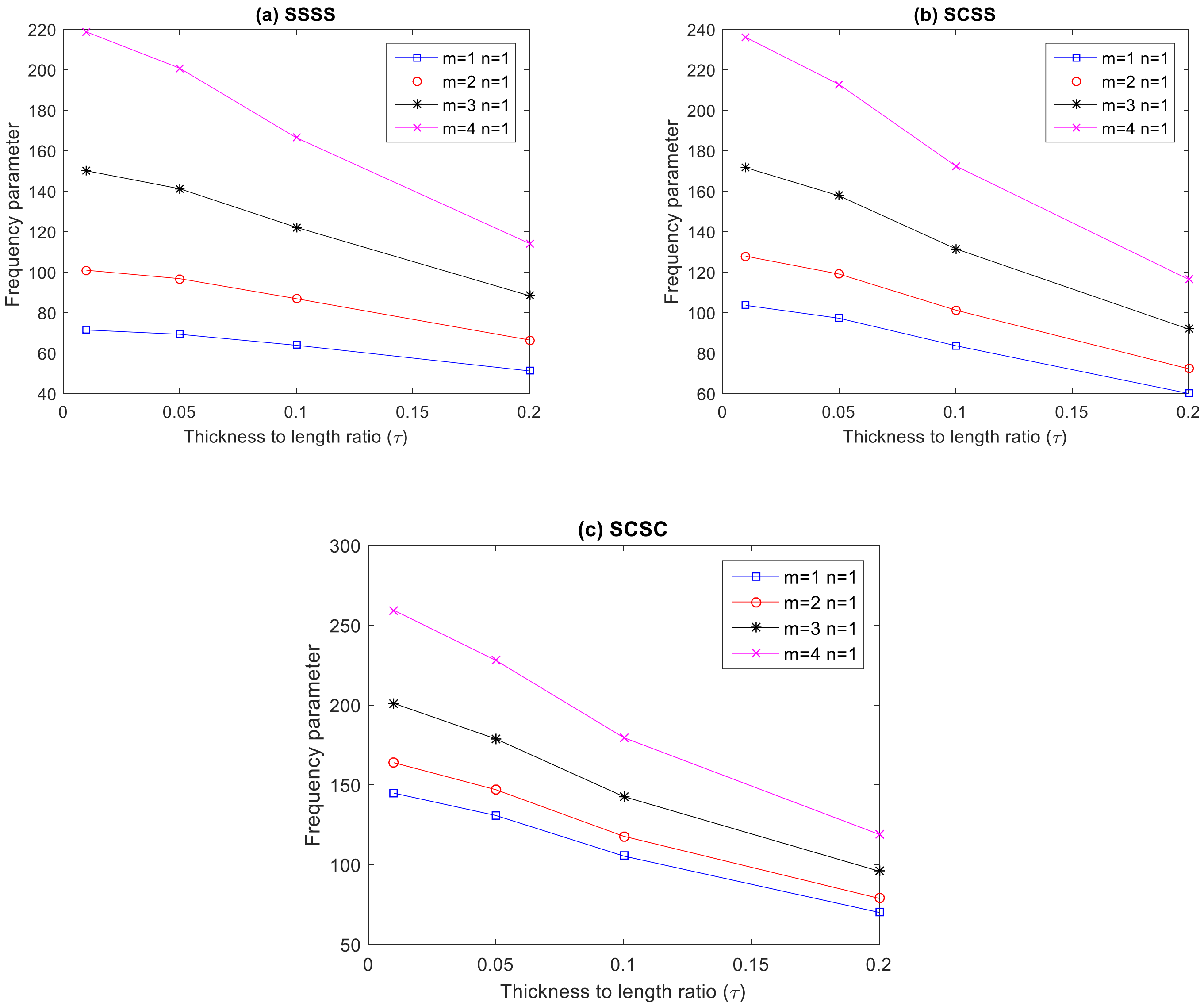

Figure 6 Variations of frequency parameter with thickness to length ratio for different modes ($\delta = 0.4$)

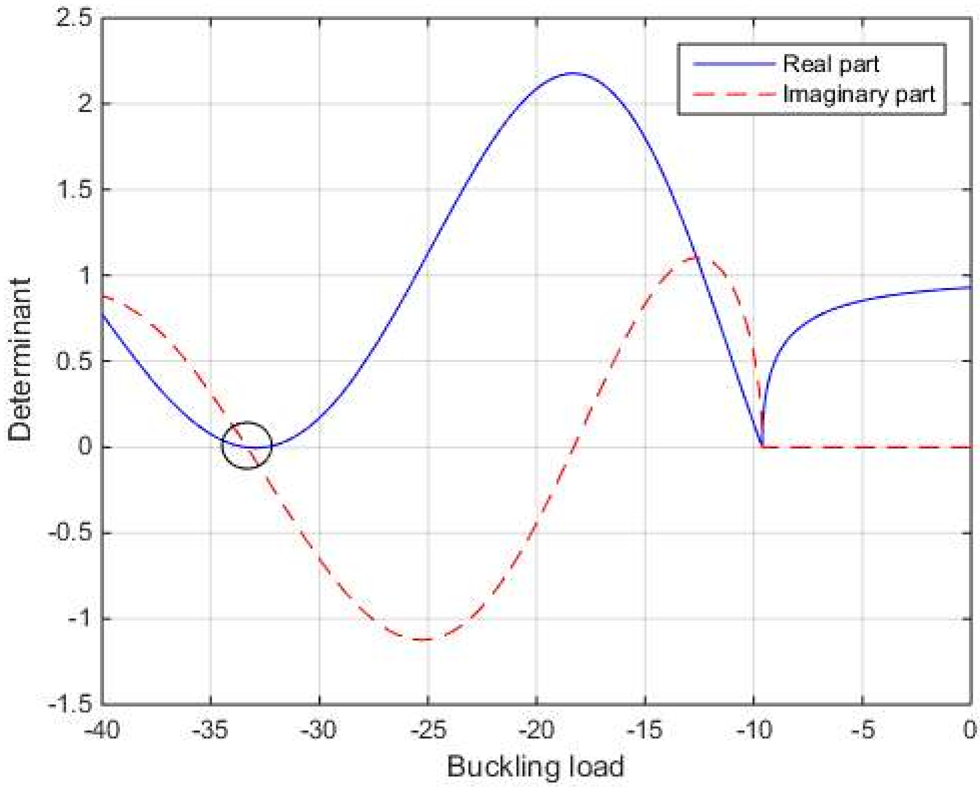

Figure *7* Real and imaginary parts of determinant of Eq. (42) ($\beta = 0$)

Table 5 *Comparison of dimensionless critical buckling load* $N = \frac{a^2}{D} N_{xx}$ *for simply supported plates*

Method	**Aspect ratio**	**Thickness to length ratio**		
		$\tau = 0.01$	$\tau = 0.1$	$\tau = 0.2$
	$\delta = 1$			
Present		**19.7281**	**18.6861**	**16.1139**
[20]		19.7285	18.7238	16.2207
	$\delta = 2$			
Present		**12.3327**	**11.9171**	**10.8148**
[20]		12.3328	11.9325	10.8641

Table 6 *dimensionless critical buckling load* $N = \frac{a^2}{D} N_{xx}$ *for different boundary conditions*

$\delta = \frac{b}{a}$	$\tau = \frac{h}{a}$	Non-dimensional critical buckling load		
	BC	SSSS	SCSS	SCSC
0.4	0.01	-71.4087	-129.6300	-237.1232
	0.05	-68.0773	-117.8268	-202.1105
	0.1	-59.4335	-92.0704	-139.0509
	0.2	-39.5356	-50.1867	-63.5075
0.5	0.01	-49.2782	- 84.8430	-150.2721
	0.05	-47.6685	-79.5633	-134.9581
	0.1	-43.2593	-66.7824	-102.7726
	0.2	-31.6290	-41.2908	-53.6786
1	0.01	-19.7281	-26.2500	-37.7476
	0.05	-19.4649	-25.7204	-36.5557
	0.1	-18.6861	-24.1988	-33.3404
	0.2	-16.1139	-19.6873	-24.9667
1.5	0.01	-14.2503	-16.3571	-19.8207
	0.05	-14.1124	-16.1562	-19.4896
	0.1	-13.6984	-15.5654	-18.5427
	0.2	-12.2621	-13.6171	-15.6381
2	0.01	-12.3327	-13.2320	-14.6103
	0.05	-12.2293	-13.1055	-14.4416
	0.1	-11.9171	-12.7278	-13.9465
	0.2	-10.8148	-11.4286	-12.3115

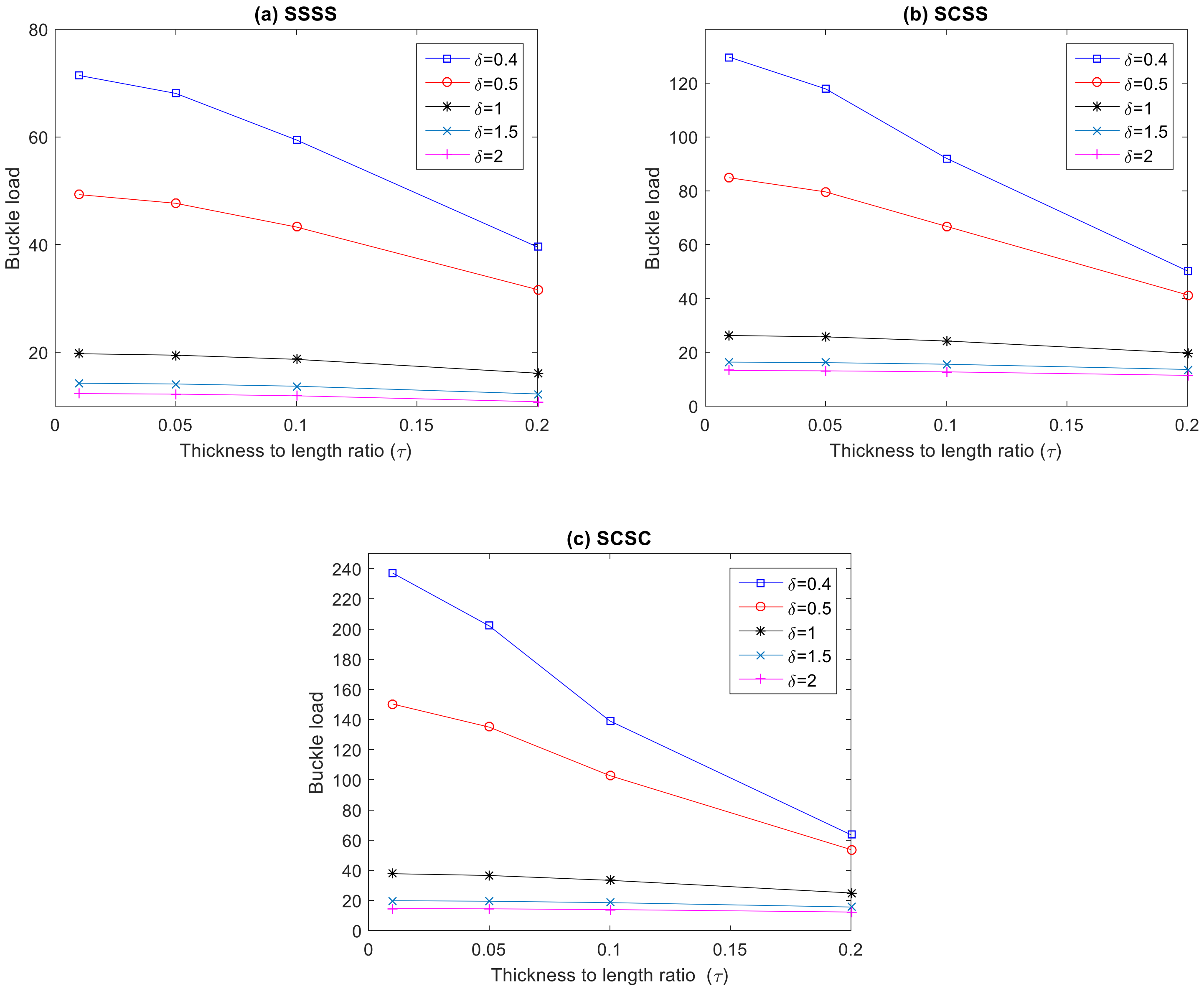

Figure 8 Variations of buckling load with thickness to length ratio for various aspect ratios

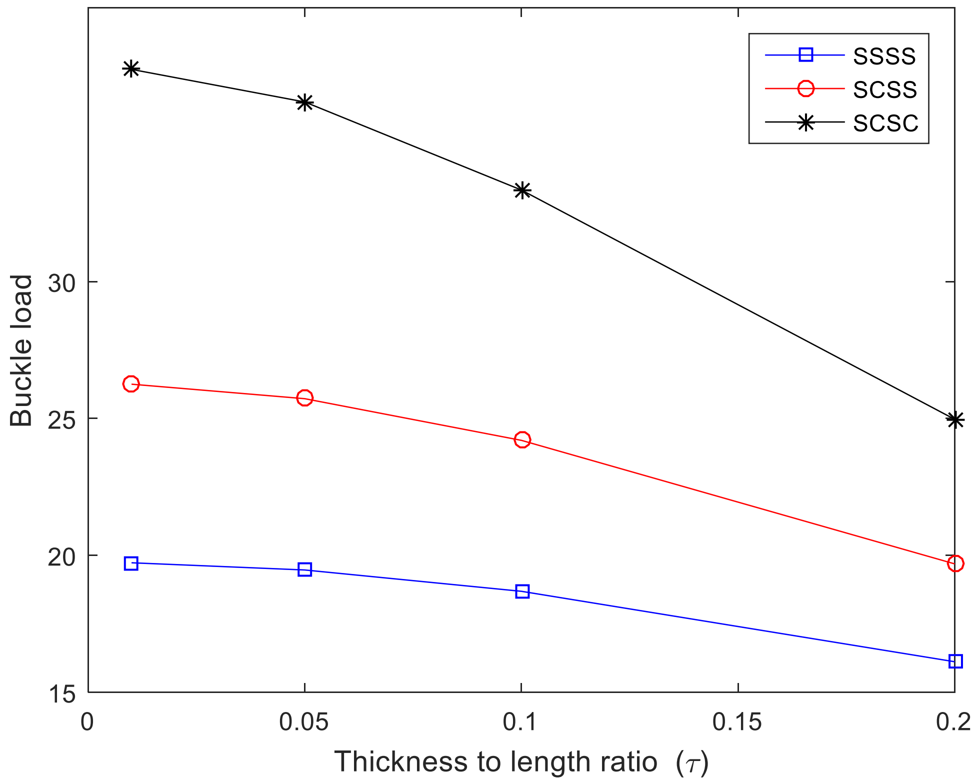

Figure 9 Variations of buckling load with thickness to length ratio for various boundary conditions ($\delta = 1$)

5. Conclusion

This paper presented free vibration and buckling analysis of the thick plates based on higher order shear deformation plate theory using wave propagation approach. Dimensionless frequencies and dimensionless buckling of the plate are compared with available results by literature that excellent agreement is observed. Benchmark results for natural frequencies and buckling loads are presented for various thickness to length ratios, aspect ratios, numbers of half waves and various combinations of boundary conditions. In future works, these results can be excellent database to verify approximate or other analytical solutions as they are regarded as exact solutions. Also, it is seen that the computer coding of the proposed method is much easier than the classical methods which makes it more appropriate in implementation.

References

[1] S. P. Timoshenko, S. Woinowsky-Krieger, 1959, *Theory of plates and shells*, McGraw-hill,

[2] R. Mindlin, Influence of rotatory inertia and shear on flexural motions of isotropic, elastic plates, *J. appl. Mech.,* Vol. 18, pp. 31, 1951.

[3] J. N. Reddy, A simple higher-order theory for laminated composite plates, *Journal of applied mechanics,* Vol. 51, No. 4, pp. 745-752, 1984.

[4] M. Zakeri, R. Attarnejad, Numerical free vibration analysis of higher-order shear deformable beams resting on two-parameter elastic foundation, *Journal of Computational Applied Mechanics,* Vol. 46, No. 2, pp. 117-131, 2015.

[5] K. Bell, A refined triangular plate bending finite element, *International journal for numerical methods in engineering,* Vol. 1, No. 1, pp. 101-122, 1969.

[6] K. Liew, F.-L. Liu, Differential cubature method: a solution technique for Kirchhoff plates of arbitrary shape, *Computer Methods in Applied Mechanics and Engineering,* Vol. 145, No. 1-2, pp. 1-10, 1997.

[7] G. Wei, Y. Zhao, Y. Xiang, The determination of natural frequencies of rectangular plates with mixed boundary conditions by discrete singular convolution, *International Journal of Mechanical Sciences,* Vol. 43, No. 8, pp. 1731-1746, 2001.

[8] C. Lü, Z. Zhang, W. Chen, Free vibration of generally supported rectangular Kirchhoff plates: State-space-based differential quadrature method, *International journal for numerical methods in engineering,* Vol. 70, No. 12, pp. 1430-1450, 2007.

[9] S. Papargyri-Beskou, D. Beskos, Static, stability and dynamic analysis of gradient elastic flexural Kirchhoff plates, *Archive of Applied Mechanics,* Vol. 78, No. 8, pp. 625-635, 2008.

[10] L. Dozio, On the use of the trigonometric Ritz method for general vibration analysis of rectangular Kirchhoff plates, *Thin-Walled Structures,* Vol. 49, No. 1, pp. 129-144, 2011.

[11] S. Shojaee, E. Izadpanah, N. Valizadeh, J. Kiendl, Free vibration analysis of thin plates by using a NURBS-based isogeometric approach, *Finite Elements in Analysis and Design,* Vol. 61, pp. 23-34, 2012.

[12] S. C. Brenner, L.-y. Sung, H. Zhang, Y. Zhang, A Morley finite element method for the displacement obstacle problem of clamped Kirchhoff plates, *Journal of Computational and Applied Mathematics,* Vol. 254, pp. 31-42, 2013.

[13] F. Millar, D. Mora, A finite element method for the buckling problem of simply supported Kirchhoff plates, *Journal of Computational and Applied Mathematics,* Vol. 286, pp. 68-78, 2015.

[14] A. Çetkin, S. Orak, The free vibration analysis of point

supported rectangular plates using quadrature element method, *Journal of Theoretical and Applied Mechanics,* Vol. 55, No. 3, pp. 1041-1053, 2017.

[15] J. Reddy, A. Khdeir, Buckling and vibration of laminated composite plates using various plate theories, *AIAA journal,* Vol. 27, No. 12, pp. 1808-1817, 1989.

[16] H.-S. Shen, J. Yang, L. Zhang, Free and forced vibration of Reissner–Mindlin plates with free edges resting on elastic foundations, *Journal of sound and vibration,* Vol. 244, No. 2, pp. 299-320, 2001.

[17] L. Qian, R. Batra, L. Chen, Free and forced vibrations of thick rectangular plates using higher-order shear and normal deformable plate theory and meshless Petrov-Galerkin (MLPG) method, *Computer Modeling in Engineering and Sciences,* Vol. 4, No. 5, pp. 519-534, 2003.

[18] S. H. Hashemi, M. Arsanjani, Exact characteristic equations for some of classical boundary conditions of vibrating moderately thick rectangular plates, *International Journal of Solids and Structures,* Vol. 42, No. 3, pp. 819-853, 2005.

[19] G. Shi, A new simple third-order shear deformation theory of plates, *International Journal of Solids and Structures,* Vol. 44, No. 13, pp. 4399-4417, 2007.

[20] S. Hosseini-Hashemi, K. Khorshidi, M. Amabili, Exact solution for linear buckling of rectangular Mindlin plates, *Journal of sound and vibration,* Vol. 315, No. 1, pp. 318-342, 2008.

[21] S. Hosseini-Hashemi, M. Fadaee, H. R. D. Taher, Exact solutions for free flexural vibration of Lévy-type rectangular thick plates via third-order shear deformation plate theory, *Applied Mathematical Modelling,* Vol. 35, No. 2, pp. 708-727, 2011.

[22] S. Eftekhari, A. Jafari, Modified mixed Ritz-DQ formulation for free vibration of thick rectangular and skew plates with general boundary conditions, *Applied Mathematical Modelling,* Vol. 37, No. 12, pp. 7398-7426, 2013.

[23] D. Shi, Q. Wang, X. Shi, F. Pang, Free vibration analysis of moderately thick rectangular plates with variable thickness and arbitrary boundary conditions, *Shock and Vibration,* Vol. 2014, 2014.

[24] K. K. Pradhan, S. Chakraverty, Transverse vibration of isotropic thick rectangular plates based on new inverse trigonometric shear deformation theories, *International Journal of Mechanical Sciences,* Vol. 94, pp. 211-231, 2015.

[25] I. Senjanović, N. Vladimir, D. S. Cho, A new finite element formulation for vibration analysis of thick plates, *International Journal of Naval Architecture and Ocean Engineering,* Vol. 7, No. 2, pp. 324-345, 2015.

[26] W. Xiang, Y. Xing, A new first-order shear deformation theory for free vibrations of rectangular plate, *International Journal of Applied Mechanics,* Vol. 7, No. 01, pp. 1550008, 2015.

[27] S. M. Mousavi, J. Paavola, J. Reddy, Variational approach to dynamic analysis of third-order shear deformable plates within gradient elasticity, *Meccanica,* Vol. 50, No. 6, pp. 1537-1550, 2015.

[28] Q. Wang, D. Shi, X. Shi, A modified solution for the free vibration analysis of moderately thick orthotropic rectangular plates with general boundary conditions, internal line supports and resting on elastic foundation, *Meccanica,* Vol. 51, No. 8, pp. 1985-2017, 2016.

[29] Y. Zhou, J. Zhu, Vibration and bending analysis of multiferroic rectangular plates using third-order shear deformation theory, *Composite Structures,* Vol. 153, pp. 712-723, 2016.

[30] P. N. Babagi, B. N. Neya, M. Dehestani, Three dimensional solution of thick rectangular simply supported plates under a moving load, *Meccanica*, pp. 1-18.

[31] R. Javidi, M. Moghimi Zand, K. Dastani, Dynamics of Nonlinear rectangular plates subjected to an orbiting mass based on shear deformation plate theory, *Journal of Computational Applied Mechanics*, 2017.

[32] H. Makvandi, S. Moradi, D. Poorveis, K. H. Shirazi, A new approach for nonlinear vibration analysis of thin and moderately thick rectangular plates under inplane compressive load.

[33] A. Daneshmehr, A. Rajabpoor, A. Hadi, Size dependent free vibration analysis of nanoplates made of functionally graded materials based on nonlocal elasticity theory with high order theories, *International Journal of Engineering Science,* Vol. 95, pp. 23-35, 2015.

[34] M. Hosseini, H. H. Gorgani, M. Shishesaz, A. Hadi, Size-Dependent Stress Analysis of Single-Wall Carbon Nanotube Based on Strain Gradient Theory, *International Journal of Applied Mechanics,* Vol. 9, No. 06, pp. 1750087, 2017.

[35] M. Hosseini, M. Shishesaz, K. N. Tahan, A. Hadi, Stress analysis of rotating nano-disks of variable thickness made of functionally graded materials, *International Journal of Engineering Science,* Vol. 109, pp. 29-53, 2016.

[36] M. Z. Nejad, A. Rastgoo, A. Hadi, Effect of exponentially-varying properties on displacements and stresses in pressurized functionally graded thick spherical shells with using iterative technique, *Journal of Solid Mechanics,* Vol. 6, No. 4, pp. 366-377, 2014.

[37] M. Z. Nejad, A. Hadi, Eringen's non-local elasticity theory for bending analysis of bi-directional functionally graded Euler–Bernoulli nano-beams, *International Journal of Engineering Science,* Vol. 106, pp. 1-9, 2016.

[38] M. Z. Nejad, A. Hadi, Non-local analysis of free vibration of bi-directional functionally graded Euler–Bernoulli nano-beams, *International Journal of Engineering Science,* Vol. 105, pp. 1-11, 2016.

[39] M. Z. Nejad, A. Hadi, A. Farajpour, Consistent couple-stress theory for free vibration analysis of Euler-Bernoulli nano-beams made of arbitrary bi-directional functionally graded materials, *Structural Engineering and Mechanics,* Vol. 63, No. 2, pp. 161-169, 2017.

[40] M. Z. Nejad, A. Hadi, A. Rastgoo, Buckling analysis of arbitrary two-directional functionally graded Euler–Bernoulli nano-beams based on nonlocal elasticity theory, *International Journal of Engineering Science,* Vol. 103, pp. 1-10, 2016.

[41] M. Z. Nejad, A. Rastgoo, A. Hadi, Exact elasto-plastic analysis of rotating disks made of functionally graded materials, *International Journal of Engineering Science,* Vol. 85, pp. 47-57, 2014.

[42] M. Shishesaz, M. Hosseini, K. N. Tahan, A. Hadi, Analysis of functionally graded nanodisks under thermoelastic loading based on the strain gradient theory, *Acta Mechanica,* Vol. 228, No. 12, pp. 4141-4168, 2017.

[43] A. Hadi, M. Z. Nejad, A. Rastgoo, M. Hosseini, Buckling analysis of FGM Euler-Bernoulli nano-beams with 3D-varying properties based on consistent couple-stress theory, *Steel and Composite Structures,* Vol. 26, No. 6, pp. 663-672, 2018.

[44] M. Zamani Nejad, M. Jabbari, A. Hadi, A review of functionally graded thick cylindrical and conical shells, *Journal of Computational Applied Mechanics,* Vol. 48, No. 2, pp. 357-370, 2017.

[45] A. Hadi, M. Z. Nejad, M. Hosseini, Vibrations of three-dimensionally graded nanobeams, *International Journal of Engineering Science,* Vol. 128, pp. 12-23, 2018.

[46] X. Zhang, Frequency analysis of submerged cylindrical shells with the wave propagation approach, *International Journal of Mechanical Sciences,* Vol. 44, No. 7, pp. 1259-1273, 2002.

[47] B. Kang, C. Riedel, C. Tan, Free vibration analysis of planar curved beams by wave propagation, *Journal of sound and vibration,* Vol. 260, No. 1, pp. 19-44, 2003.

[48] T. Natsuki, M. Endo, H. Tsuda, Vibration analysis of embedded carbon nanotubes using wave propagation approach, *Journal of Applied Physics,* Vol. 99, No. 3, pp. 034311, 2006.

[49] S.-K. Lee, B. Mace, M. Brennan, Wave propagation, reflection and transmission in curved beams, *Journal of sound and vibration,* Vol. 306, No. 3, pp. 636-656, 2007.

[50] M. N. Bahrami, M. K. Arani, N. R. Saleh, Modified wave approach for calculation of natural frequencies and mode shapes in arbitrary non-uniform beams, *Scientia Iranica,* Vol. 18, No. 5, pp. 1088-1094, 2011.

[51] A. Bahrami, M. R. Ilkhani, M. N. Bahrami, Wave propagation technique for free vibration analysis of annular circular and sectorial membranes, *Journal of Vibration and Control,* Vol. 21, No. 9, pp. 1866-1872, 2015.

[52] A. Bahrami, A. Teimourian, Nonlocal scale effects on buckling, vibration and wave reflection in nanobeams via wave propagation approach, *Composite Structures,* Vol. 134, pp. 1061-1075, 2015.

[53] A. Bahrami, A. Teimourian, Free vibration analysis of composite, circular annular membranes using wave propagation approach, *Applied Mathematical Modelling,* Vol. 39, No. 16, pp. 4781-4796, 2015.

[54] A. Bahrami, A. Teimourian, Small scale effect on vibration and wave power reflection in circular annular nanoplates, *Composites Part B: Engineering,* Vol. 109, pp. 214-226, 2017.

[55] A. Bahrami, A. Teimourian, Study on vibration, wave reflection and transmission in composite rectangular membranes using wave propagation approach, *Meccanica,* Vol. 52, No. 1-2, pp. 231-249, 2017.

[56] A. Bahrami, A. Teimourian, Study on the effect of small scale on the wave reflection in carbon nanotubes using nonlocal Timoshenko beam theory and wave propagation approach, *Composites Part B: Engineering,* Vol. 91, pp. 492-504, 2016.

[57] M. Ilkhani, A. Bahrami, S. Hosseini-Hashemi, Free vibrations of thin rectangular nano-plates using wave propagation approach, *Applied Mathematical Modelling,* Vol. 40, No. 2, pp. 1287-1299, 2016.

[58] A. Bahrami, Free vibration, wave power transmission and reflection in multi-cracked nanorods, *COMPOSITES PART B-ENGINEERING,* Vol. 127, pp. 53-62, 2017.

[59] A. Bahrami, A wave-based computational method for free vibration, wave power transmission and reflection in multi-cracked nanobeams, *Composites Part B: Engineering,* Vol. 120, pp. 168-181, 2017.